Design and implementation of Personal Computer based data acquisition and analysis in electrochemical and solid state areas.

B D J R Fennema

M Sc 1992

Design and implementation of Personal Computer based data acquisition and analysis in electrochemical and solid state areas.

B D J R Fennema (M Sc Chem.)

Submitted for the degree of Master of Science

Supervisor Dr G Hughes, School of Physical Sciences, Dublin City University, Glasnevin, Dublin 9

Submitted November 1992

I hereby declare that this thesis has been based on my own work and has not been submitted elsewhere

Boris Fennema

Boris Fennema

For Eithne, Koos and Fokke

Abstract

The original aim of this project was to investigate how the electrochemical activity of polymer modified electrodes depends on the polymer morphology and the structure of the polymer-electrode interface In principle, the use of these mediating layers on electrode surfaces make it possible to control the properties of the interface at a molecular level Firstly, the methods of data acquisition and analysis used to extract fundamental parameters of the redox polymer concerning charge transfer characteristics have been put under PC control This facilitates a more systematic approach to the data acquisition and analysis as compared to the methods used before Secondly, surface science techniques have been used in an attempt to determine the chemical composition and physical structure of the polymer layer and to establish whether the surface composition was dependent on the electrochemical treatment of the polymer modified electrode During the progress of this project, the expertise gained during the first instrumentation oriented stage has been extended towards capacitance measurements on solid state systems

List of symbols

Symbol	Meaning	Dimensions
$_r$	species r in O + ne <-> R	
$_o$	species O in O + ne <-> R	
$_p$	peak	
A	Area	cm^2
C	Capacitance	F,μF
C_j	Concentration of j	mol/cm^3
D_α	Diffusion coefficient	cm^2s
E_o	Formal electrode potential	V
$E_{½}$	Reversible half wave potential	
	$E_{½} = E_o + RT \ln(D_r/D_o)^{½}$	V
F	Faraday constant	C
i,I	Current	A
Im	imaginary part of complex number	
k	rate constant	depends
N_d	electron density in semiconductor	cm^{-3}
n	number of electrons in reaction	unity
Q	charge	C,μC
R	a) gas constant	$J\ mol^{-1}\ K^{1}$
	b) Resistance	Ohms
Re	real part of complex number	
T	absolute temperature	K
t	time	s
V_{fb}	flatband potential	V
X	reactance	Ohms
Z	impedance	Ohms
α	transfer coefficient	none
Γ	surface coverage	mol/cm^2
ε	dielectric constant	none
Θ	angle	radians
ω	angular frequency	radians/s

List of abbreviations

ADC	analog-to-digital converter
DAC	digital-to-analog converter
EXAFS	extended X-ray absorption edge fine structure spectroscopy
FFT	fast Fourier transform
GPIB	general purpose interface bus
IS	impedance spectroscopy
LIA	lock-in amplifier
PC	personal computer
PME	polymer modified electrode
RMS	root mean square
STM	scanning tunnelling microscope
XPS	X-ray photoelectron spectroscopy

Index

Chapter 1

Design and implementation of Personal Computer based data acquisition and analysis in electrochemical and solid state areas

1.1. Introduction.

The original aim of this multi-disciplinary project was to investigate how the electrochemical activity of polymer modified electrodes (PME's) depends on the polymer morphology and the structure of the polymer-electrode interface. The metal loaded polymer coatings studied in this project mediate the charge transfer between electrode and electrolyte at the reduction and oxidation potential of the metal present m the polymer. In principle, the use of these mediating layers on electrode surfaces make it possible to control the properties of the interface at a molecular level [1] The electrochemical nature of the layer therefore determines the precise charge transfer characteristics of the interface The experimental approach adopted was to divide the project in to three separate but interrelated phases aimed at obtaining a systematic understanding of the kinetic parameters which determine the charge transfer processes taking place across the polymer layer

In the first phase, to enable us to collect and process the data more efficiently,the existing analog electrochemical equipment has been interfaced to a personal computer The second phase consists of systematically characterising the PME's charge transfer properties using the instrumentation developed From the subsequent data analysis information concerning the charge transfer processes would then be accessible [2,3]

We also attempted to use semiconductor as possible electrode material. This would yield additional control over the charge transfer between substrate and modifying layer as explained in Chapter 5 in more detail

The final phase of the project involves investigation and analysis of surface composition and structure of the PME by means of scanning tunnelling microscopy (STM) and X-ray photon electron spectroscopy (XPS) If possible, the data obtained from this step would be correlated with the charge transfer data obtained in the second phase

1.2 Aims and objectives of the project

The main objectives of this project have been twofold

1) design and implementation of instrumentation needed in order to be able to measure and evaluate the electrochemical and electronic characteristics of the PME's
2) if possible,link the information obtained to the morphology , or more specific the surface structure of these materials as investigated using STM/XPS

As will be discussed in more detail in Chapter 5, the proposed semiconductor-redoxpolymer device exhibited serious stability problems in the investigated electrolytes, making any kind of investigation of the electrochemical and electronic properties of these materials extremely cumbersome and prone to irreproducibility. Therefore, we have concentrated our efforts on accumulating the electrochemical measurements in a more reproducible and efficient manner Hence, the main emphasis of this project became the design and implementation of PC based data acquisition and analysis in electrochemical techniques, which was subsequently extended towards developing semiconductor solid state instrumentation complementary to the existing characterisation techniques available in Dublin City University This involved variable frequency impedance spectroscopy (Chapter 3 and 4), which is a useful technique in the study of semiconductor Schottky diodes

1 3 Lay Out of the thesis

The work described here covers the next 5 chapters The following chapters describe the instrumentation and software developed in phase 1 of this project in more detail Chapter 2 deals with the implementation of data acquisition and analysis software to improve and enhance the existing analog electrochemical equipment. Chapter 3 and 4 describe the instrumentation which performs variable frequency capacitance measurements, used to characterise solid state devices Chapter 3 gives a brief introduction into the generic technique of impedance spectroscopy and details of the design and schematics of the hardware and software necessary to implement the single frequency approach to measure capacitance. Also in Chapter 3 an overview of the calibration and validation procedure of the final setup is presented. Chapter 4 describes an typical experiment and briefly demonstrates one area where the technique as implemented here fails to produce consistent results. Chapter 5 includes the preliminary results and reports on the outcome of the various electrochemical and surface analysis experiments carried out in this project The thesis concludes with Chapter 6, in which a brief overview of the work described is combined with suggestions for future activities.

References

1 a) R W Murray et al , Anal Chem , 59,379-390,1987
b) R W Murray, Acc Chem.Res , 13, 135-141, 1980

2 H Matsuda, Bull Chem Soc Jpn , 53, 3439-3446, 1980

3 A.J. Bard and L R Faulkner, Electrochemical Methods, Wiley, 1980 Chapters 3,4,5 and 9 in particular

Chapter 2

Design and implementation of a data acquisition and analysis system to be used for specialised electrochemical studies

2 1. Introduction

Electrochemical measurements such as those carried out on polymer modified electrode systems studied in the Chemistry Department at D.C U impose a large amount of data acquisition and post-run analysis on the experimenter.

In this specific case, settings on the equipment used (potentiostat in conjunction with a chart recorder and/or oscilloscope) have to be altered between the basic set of experiments used for each sample. Done manually this is tedious, repetitive and prone to operator error. Furthermore, chart recorder technology requires a lot of cut and paste manoeuvres to be carried out to obtain the raw data after which lengthy calculations take over Another drawback is that the scientific quality is not equalled by presentability of the results For publications or presentations, one may have to redraw the data by hand on tracing paper in order to obtain good quality figures In short, analogue equipment is excellent for generating the data, but fails to deliver on the analysis and presentation of data. Also, changing from one experimental setup to another involves assistance of the operator

Digital technology renders the advantages of hardware control (ease of setting the instrument up for a specific experiment using default or stored settings), manipulation, storage and analysis of the data obtained It also allows for the use of desk top publishing (DTP) packages for high quality output by importing the data in ASCII format into a spreadsheet or word processor (Figure 2.1).

The new generation of digital technology based potentiostat is capable of being computer controlled and hence gives rise to the advantages mentioned above. However, they are expensive and the software shipped with this type of equipment is usually rigid and although excellent for general use electrochemistry, it is not tailor made for a specific application

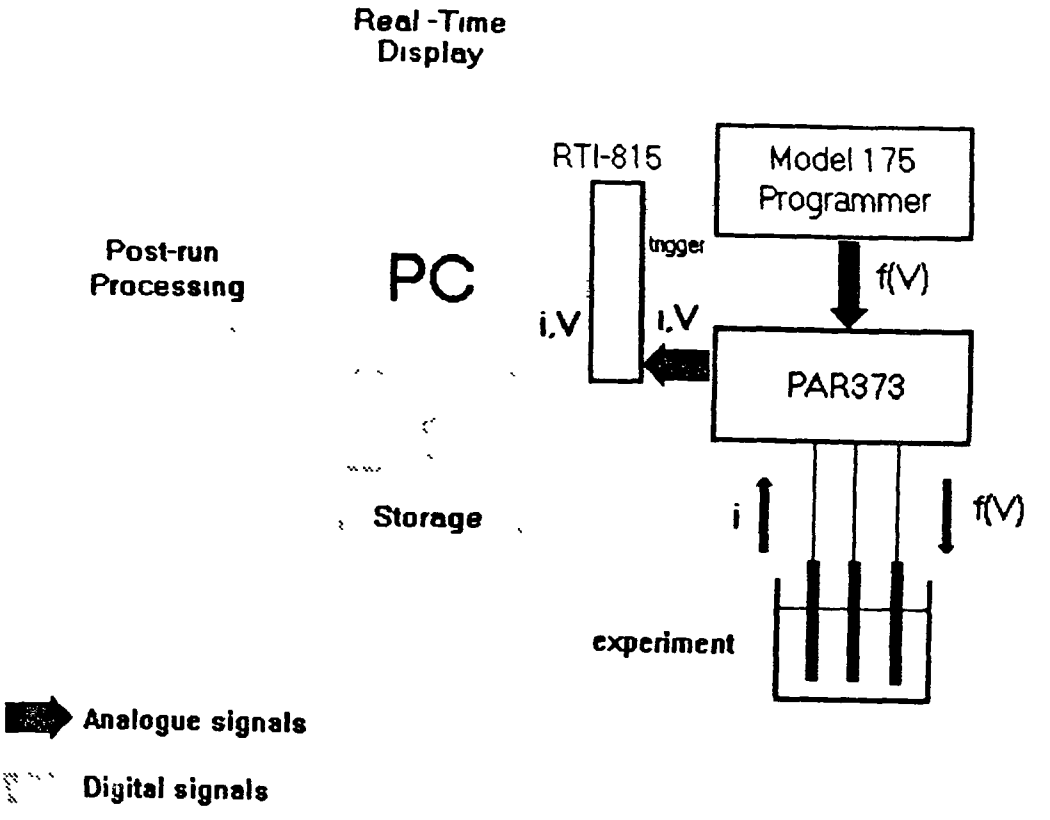

Figure 2.1. Schematic of the instrumentation layout Voltage scans from the EG&G programmer (Model 175) are triggered by the PC *via* one of the RTI-815 digital I/O lines and the current/voltage (I/V) data captured from the EG&G 363 potentiostat using two analogue-input channels The digitised data is available for post-run analysis and processing using in-house developed routines or for export in ASCII format to spreadsheets or other application software

This is why we choose a personal computer (PC) based data acquisition and analysis system built around a analogue potentiostat This approach would give us a hybrid system with a maximum of benefits

Three different electrochemical techniques commonly used in the study of polymer modified electrodes (PME's) were chosen as a possible data acquisition and analysis system The next section intends to give a brief introduction on the synthesis and properties of the PME's used in this project

The methods used in a typical PME study are cyclic voltammetry, sampled current voltammetry and chronoamperometry All these techniques have their specific experimental setup parameters and post-run analysis requirements,

as described in following sections These sections will include specifications and details of software and calculations used in the analysis procedures Some details concerning the I/O card used as link between instrument and software will be presented in section 2 6 of this chapter

2 2 Electrochemical background and introduction to PME's

Electrochemical reactions take place at the electrode/electrolyte interface. A greater understanding in the charge transfer processes that occur at these interfaces have implications for sensory devices or electrocatalysts, which depend on charge transfer mechanisms Due to the great importance of the interface in electrochemical processes, one would like to have direct control over the chemical and physical structure of the interface in order to be able to design this boundary on a molecular level. This is the area of Chemically Modified Electrodes (CME) or its sub-class, the polymer modified electrode (PME) Polymer modified electrodes as studied at D.C.U have the advantage of synthetic flexibility in designing a particular polymer to modify the electrode surface [1]. The polymer used in PME's chosen for this project is $[Os(bpy)_2(PVP)_{10}Cl]Cl$ (bpy=2,2'-bipyridine, PVP=poly-4-vinyl-pyrididine) A schematic drawing of this polymer is presented in Figure 2 2 overleaf. The starting materials $Os(bpy)_2Cl_2$ and the polymer are prepared using standard techniques [2] The first step is to dissolve the osmium salt in a high boiling solvent such as methoxy-ethanol under reflux, after which a 10 mole equivalent amount of the polymer is added in portions Due to the fact that the formation of the chelate is kinetically sluggish (even with the use of a high boiling alcohol) the resulting mixture is heated under reflux for a minimum of 72 hours The oxidation potentials for the osmium(II/III) redox centre as in the starting material and the polymer product are distinctly different and this can be employed to monitor the reaction Thermodynamically the chelate formation is favoured and therefore the reaction will go towards completion The redox polymer is precipitated by adding ethoxyether to the cooled down reaction mixture and filtration yields the desired product in high yields (>90%) The PME's are fabricated by evaporation of 10 µl of a 1mg/ml solution of the polymer in methanol on the appropriate substrate under vacuum.

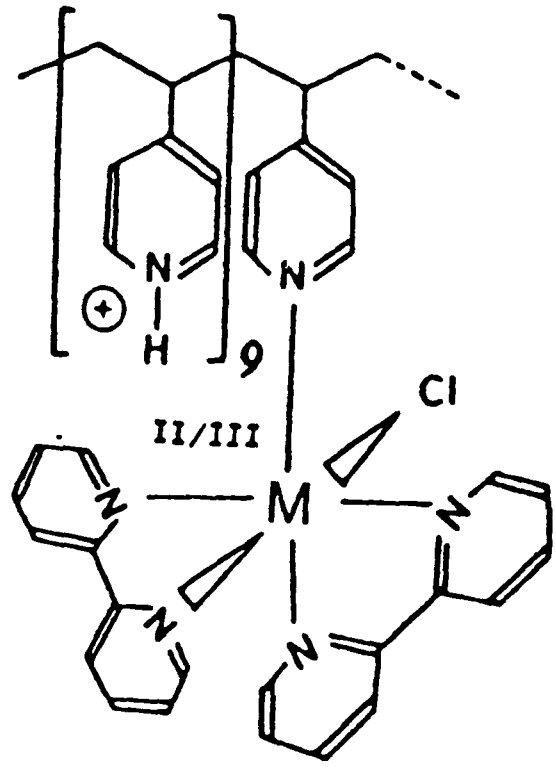

Figure 2.2 Schematic representation of $[Os(bpy)_2(PVP)_{10}Cl]Cl$ (bpy=2,2'-bipyridine, PVP=poly-4-vinyl-pyrididine). The metal ion M is Os(II/III) Note the 1:10 ratio results in 9 free pendant pyridine for every occupied moiety.

Charge transfer is a fundamental process occurring in all electrochemical processes [3] For PME's there are three regions of interest, the electrode-film interface, the polymer itself and the film-electrolyte interface. The homogeneous process arises within the redox polymer matrix upon instantaneous injection of electrons from the metallic electrode surface into the film, while the heterogeneous mechanism provides a gateway at the film-electrolyte interface Based on this model there are three parameters k_o, D_{ct} and α (see Figure 2.3) experimentally accessible, using the following techniques

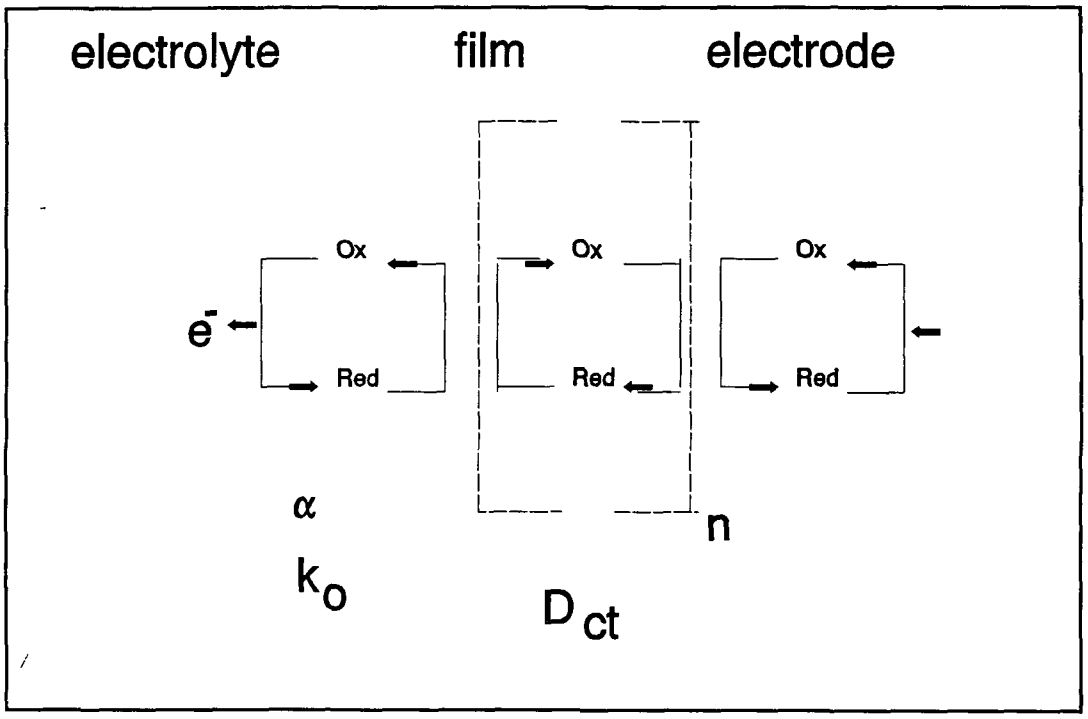

Figure 2.3 Schematic presentation of the heterogeneous and homogeneous charge transfer parameters for an anodic process across an electrode-film-electrolyte interface

Cyclic voltammetry provides information concerning the homogeneous charge transfer process (D_{α}) in combination with parameters concerning the physical properties of the film (layer thickness estimate and stability over time) The D_{α} parameter has the significance and dimensions of a diffusion coefficient, describing the charge transport through the film Sampled current voltammetry gives details on the heterogeneous aspect of the charge transfer (k_0 and α) at the film-electrolyte interface Chronoamperometry is used to study the homogeneous mechanism under pulse conditions instead of a relatively slow voltage ramp as used in cyclic voltammetry. More details on experimental conditions will be given in the following sections

2 3 Cyclic Voltammetry

2.3 1 Description of the technique

In this type of experiment a triangular voltage ramp is applied to the system while monitoring the current response Sweep rates that are used in conventional studies are in the order 1 mV/s- 1 V/s When slow sweep rates are used (<5mV/s) one establishes what is known as a finite diffusion regime This means that the changes in potential are occurring at such a time scale that the whole layer experiences the effect of the potential applied before the bias is changed Theoretically the peak current i_p measured for a voltammogram obtained under these experimental conditions obeys the equation 2 1 [3]

$$i_p = \frac{\nu n^2 F^2 \Gamma}{4RT} \qquad (2.1)$$

with n the number of electrons taking part in the process, Γ the surface coverage and ν the sweep rate (all other symbols have their usual meaning) Also there should be no separation between the oxidation wave and reduction wave Γ is the total amount of electro-active material present at the electrode surface, which can be calculated using $\Gamma = Q/nFA$,where Q is the total charge passed upon oxidation or reduction (= area under respective wave) and all other symbols have their usual meaning.

Therefore two important parameters can be obtained from a voltammogram measured at low sweep rates, the total surface coverage Γ (if the peak-to-peak separation is non-zero this is only a estimate) and the peak-to-peak separation If this separation does not go to zero at low sweep rates this can be an indication of films that are too thick (finite diffusion state is not being reached for the whole of the film) or very slow heterogenous kinetics across the electrode-polymer interface, apart from experimental errors such as electrodes too far apart, or potential drops due to high resistance media and/or long conductance paths in the cell (iR drop)

At higher sweep rates one forces a semi-infinite diffusion regime upon the system under investigation

This means that the potential is altered on a time scale that only a certain fraction of the film can respond to this change in bias Therefore the Γ measured under those conditions will be significantly lower than the value obtained at low sweep rates (infinite diffusion) and the oxidation and reduction peak will be separated by several tenths of mV dependent on sweep rate and temperature For semi-infinite diffusion the Randles-Sevçik equation applies (A is surface area) [4]

$$i_p = \frac{0.4463\,(nF)^{3/2} A C_o \sqrt{\nu D_{ct}}}{\sqrt{RT}} \qquad (2.2)$$

According to this equation a plot of peak current i_p versus $v^{1/2}$ (the square root of the sweep rate) is linear and a value for the homogeneous charge transfer coefficient D_α can be evaluated This relationship only holds under semi-infinite diffusion *i e* sweep rates of 0 1-0 5 V/s for the materials studied in the Chemistry Department in D C U. An example of this type of behaviour can be seen in Figure 2 4 which shows the effect of sweep rate when measuring linear sweep voltammograms.

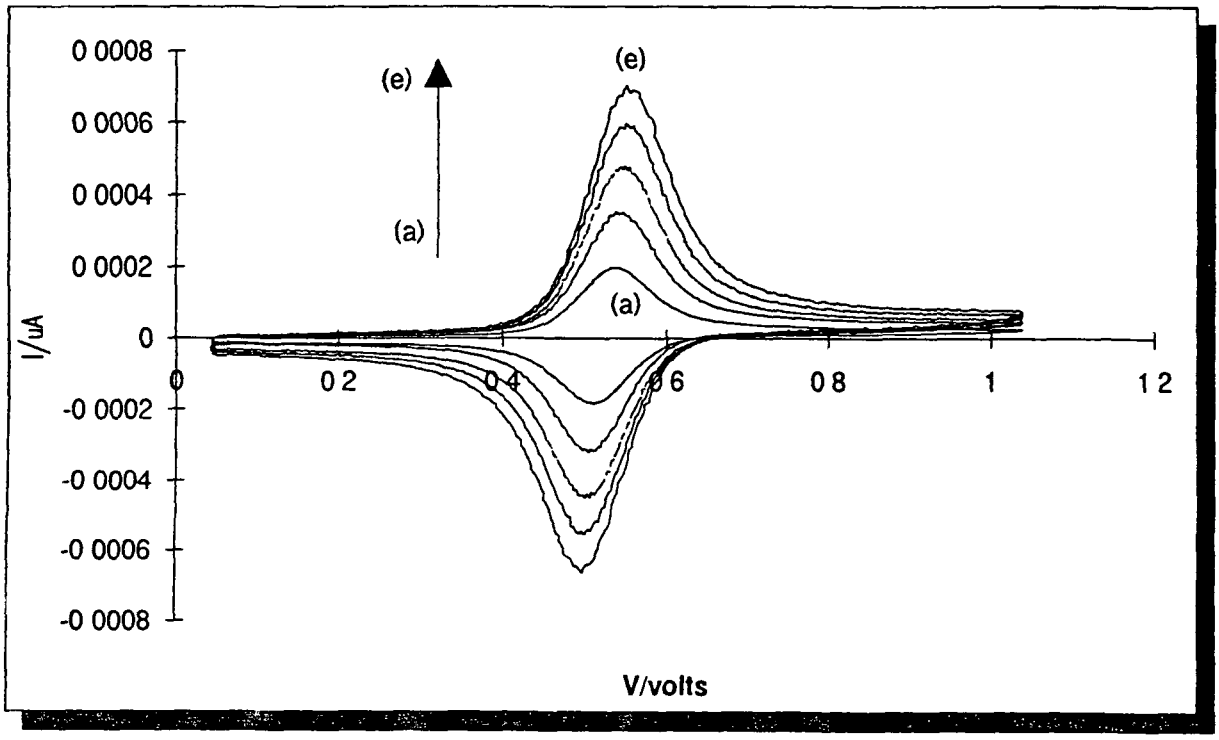

Figure 2.4 The effect of scan rate (100-500 mV/s, (a)-(e)) on an Os(II/III) redox couple present in a $[Os(bpy)_2(PVP)_{10}Cl]Cl$ polymer film on a glassy carbon substrate with 0 1 molar toluene sulphonic acid as supporting electrolyte The diagram has been constructed by importing the digitised data into MicroSoft Excel

2 3 2. Specifications

The software had to be capable of acquiring cyclic voltammograms over the sweep range specified above (1 mV/s - 0 5 V/s) at the maximum resolution of the I/O card (2 44 mV) Under software control the potentiostat mode could be set at either continuous sweep (for conditioning the films) or single sweep mode, all other settings (start and stop potential and current range) being set manually. Post-run analysis consists of integration of the peak area and verification of Sevçik's model. Other features include the facility of making overlay plots and a smooth procedure

2 3 3 Data acquisition details

Data accession can either be triggered (using the pulse function of the I/O card in combination with a pulse inverter IC), or continuous with a specified time interval between the digitised scans and guided by using real time plotting using VGA Graphics At the heart of the program are effectively two loops. The outer loop controls the total number of data points taken in order to achieve maximum resolution as given by (2*sweep window)/2.44 mV (2 44 mV is the ADC's resolution) Each data point consists of a voltage and current value stored in a binary record structure The outer loop also has to check whether a key has been pressed in order to abort or alter any of the data acquisition settings It achieves this by employing the following pseudo-code

```
While Not Abort Or Finished Do Begin
    If KeyPressed Then
        DecideOption (* sets options*)
    Else
        Inner loop   (* measure & display *)
end (* while *)
```

Using this high level checking for key presses is far easier to implement than interrupt driven routines and does not affect the real-time display abilities of the program up to scan rates of 1 V/s The inner-loop (in pseudo code) is implemented as follows.

```
For Counter.= 1 To Average Do Begin
      VoltageBit:=VoltageBit+ ADC_BitCount  (* Channel 0 *)
      CurrentBit.=CurrentBit+ ADC_BitCount  (* Channel 1 *)
END
```

and inside the outer loop the bit numbers obtained are averaged and converted to their corresponding 'real world' values As can be seen from the pseudo code, data from the 2 channels is logged continuously within the inner loop and the sweep rate determines how often the summed bit numbers are converted into data inside the outer loop. This part of the program is 'tuned' for a 80286 (PC-AT) running at 13 MHz

2 3.4. Analysis software details.

This procedure can be used to evaluate the homogeneous charge transfer coefficient D_{ct} from the anodic current i_0 vs (scan rate)$^{1/2}$ at 25° Celsius using the Sevçik relationship The general expression is given by:

$$i_p = \frac{0.4463\,(nF)^{3/2} A C_o \sqrt{v D_{ct}}}{\sqrt{RT}} \qquad (2.3)$$

Or at 293 K, the area A in cm^2, D_{ct} in cm^2/sec, C_0 in mole/cm^3, v in V/sec and i_p in amps:

$$i_p = 2.69 \times 10^5 n\sqrt{n} A \sqrt{(D_{ct} v)}\, C_o \qquad (2.4)$$

The user is prompted to give values for initial and final potential, scan rate and concentration of electro-active species. Having entered these parameters, the data will be plotted and the user has to set two respective windows and perform two back ground corrections (forward and reverse wave) by using the arrow-keys (more details can be found elsewhere [5]) The analysis routine employs Simpson's rule for integration and returns the following parameters oxidation/reduction potential, peak-to-peak separation and peak currents corrected for the background current and area under the respective waves

Smoothing of raw data is achieved by using a Savitsky-Golay 5 point moving window algorithm [6]

2 4 Sampled Current Voltammetry

2 4.1. Description of the technique.

In this experiment a pulse train is applied to the system under study and the current response is monitored A typical pulse train is depicted schematically in Figure 2.5.

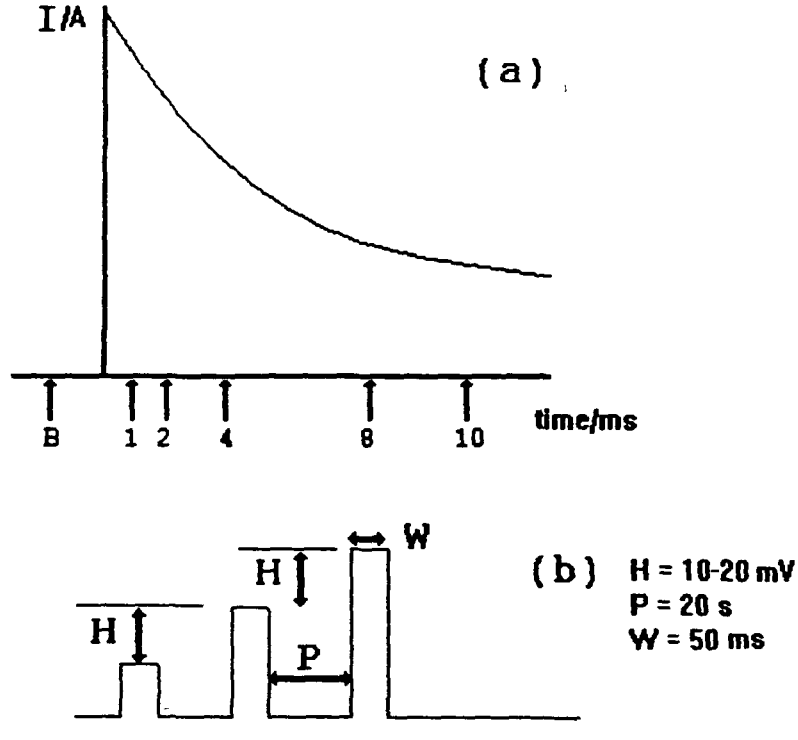

Figure 2.5 Current sampling points (a) and pulse train details (b) used in sampled current voltammetry. The sample is subjected to a voltage pulse every 20 seconds (pulse width 50 ms) with the pulse height being stepped up by a fixed step (10-20 mv) The current response is sampled just before the pulse is applied (B) for back ground correction, and then at 1,2,4,8, and 10 ms after the pulse is triggered

When the system is excited by a pulse which reaches a value located around the half-wave potential ($E_{1/2}$) value for the particular redox couple present, a current transient will be induced. In sampled current voltammetry this transient is captured

and sampled at various time intervals [7] In this example, the transient is captured over 40 ms using the parallel data transfer facility of the RTI-815 card and the sampling is carried out at 1, 2, 4, 8 and 10 ms after excitation of the redox system, as measured from the onset of the pulse A plot of the resulting time-current data is presented in Figure 2 6 (overleaf) and shows the typical sigmoidal response of the redox couple Three distinct regions can be identified, the first region being the non-active section at potentials below the half-wave potential ($E_{1/2}$) Data from this part of the curve is used to calculate the back ground correction as explained later At potentials above the half-wave potential a steady state response is reached as shown by the level section at the right hand side of the curve The sloping part between these two regions is used to calculate the heterogeneous charge transfer parameters k_o and α This is accomplished as outlined in section 2 4 4 and involves transforming the digitised data using a logarithmic function

2 4.2 Specifications

In this case the software has to be able to generate the pulse train and capture the current trace employing Direct Memory Access (DMA) for correct timing Sampling of the trace is carried out between pulses and data is stored in a binary format The program has complete hardware control over the experimental setup except for current range selection The analysis routines involve a complicated line of linear regression and background correction routines as described below

2 4 3 Data acquisition software details

The software allows the user to change settings such as total number of pulses applied (*via* the pulse height) and pause duration in between pulses during data acquisition The operator is guided by the Real Time plotting of the raw data and is able to abort the acquisition at any time during the scan Also the program checks whether the proper current range is selected by applying the largest pulse step to the system and after 1 ms delay the channel on which the current transducer is bemg monitored is checked for a value below the maximum output voltage of the transducer (2 V for the 363 EG & G PAR model used) The pulse train is generated by setting the DAC to the respective voltage level, while using the millisecond delay function of Turbo Pascal 6 0 to time pulse width and delay between pulses DMA (on the I/O board) is used to capture the trace and data is being processed in the pause sequence between pulses

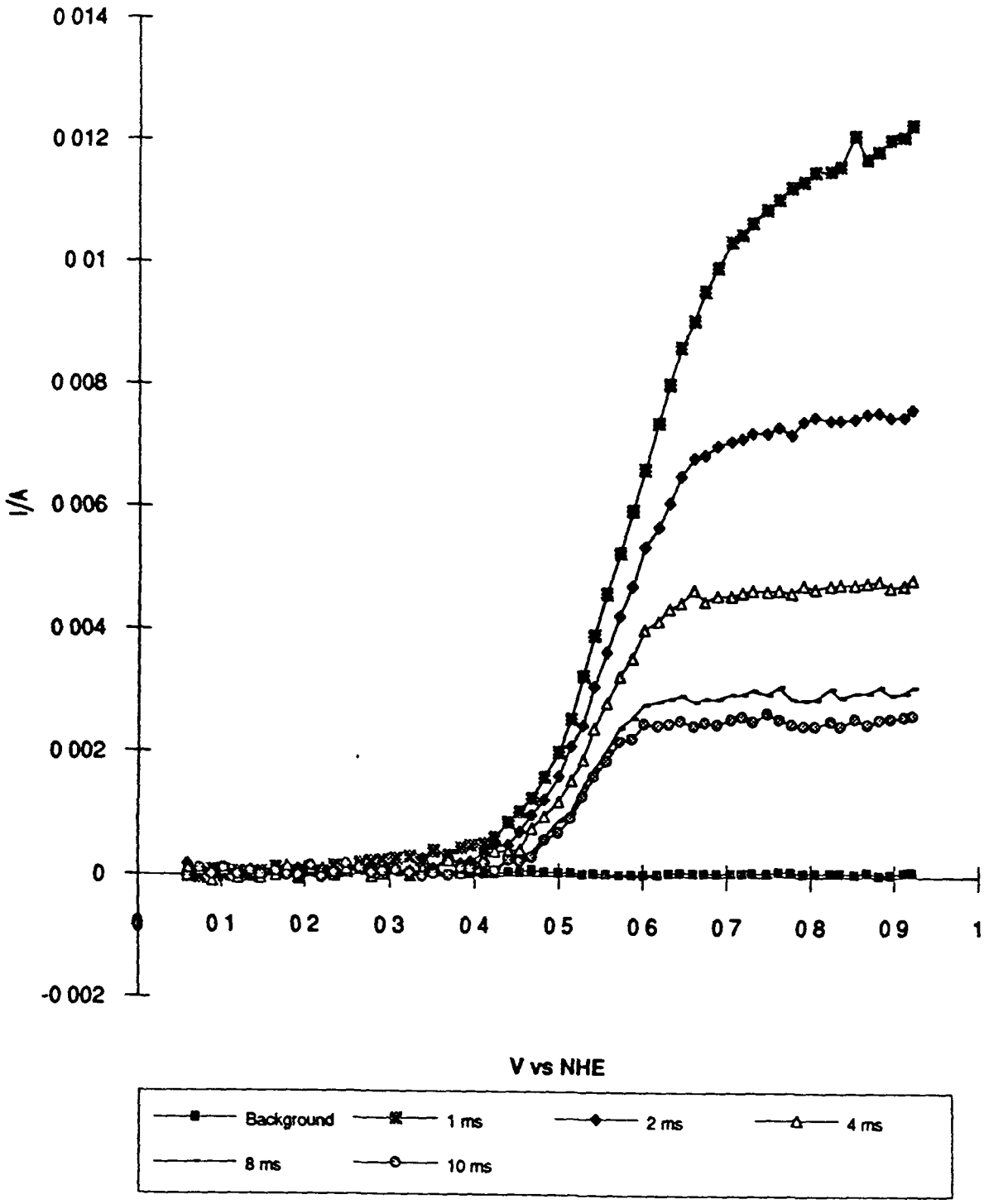

Figure 2.6 A pulse train consisting of 60 pulses were applied to an osmium(II/III) couple present as an $Os[PVP]_{10}Cl$ polymer film on a glassy carbon substrate with aqueous 0 1 molar toluene sulphomc acid as supporting electrolyte

2 4 4 Analysis software details

Parameters concerning heterogeneous charge transfer (across the electrode substrate) can be obtained by following Matsuda's approach as follows

After entering the following parameters (e g temperature, electrode diameter, number of electrons involved and the concentration of the active species) the recorded data is displayed on the screen in terms of current transients acquired at 1,2,4,8,10 ms after excitation of the sample, together with the background current trace. The standard electrode potential (E_0) value can either be fixed at the value obtained from voltammetry at low sweep rates, or evaluated from the selected pulse window, using a 5 point Savitsky-Golay second-order derivation algorithm to find the point of inflection m the rising section of the acquired data (i.e. $d^2(x)/d^2(Eappl)$) Background correction is applied based on linear regression of non-sloping section of the data located at potentials below the half-wave potential, assuming a linear response of background with applied potential, this means that the residual current is assumed to be directly proportional to the potential difference applied (*e g* V:=IR, Ohm's law). The first step in the analysis of the data is based on the Cottrell equation (Eq.2 5) [8]

$$i(t) = \frac{nFAC_o\sqrt{D_{ct}}}{\sqrt{\Pi t}} \qquad (2.5)$$

where i(t) is the current at time t, F the Faraday constant, n the number of electrons, A the electrode surface area (in cm^2), C_0 the concentration of the electroactive species in the bulk solution ($moles/cm^3$), D_{ct} the diffusion coefficient, and t the sampling time

The analysis consists of a plot of current i(t) vs $1/t^{1/2}$ with t the sampling time in seconds which gives a line of slope proportional to $\sqrt{D_{ct}}$, with all factors contributing to the proportionality constant known Hence, from this plot the diffusion coefficient D_{ct} (cm^2s^{-1}) may be evaluated The data used are the 5 points located at the plateau current where the applied potential is greater than the half-wave potential

Using Matsuda's approach [9] and the assumption that the diffusion coefficients for oxidation and reduction are identical, the transfer coefficient (α) and the heterogeneous rate constant (k_o) can be determined The transfer coefficient is the fraction of reduced species, and is similar to a symmetry factor describing which process is favoured, oxidation or reduction (for an ideally reversible reaction α should be 0.5) The heterogeneous rate constant gives the rate at which electrons can cross the electrode-electrolyte junction, or more specifically the electrode-polymer interface. The data measured at potential close to the half-wave potential is now used to calculate these parameters k_o and α Therefore the data has to be transformed into a dimensionless logarithmic format as explained in reference [9]. As one can see from the rather elaborate expression (Equation 2.6), this would be hard without digitised data and the transfer coefficient α is calculated from plotting·

$$E_{appl} \quad vs \quad \ln\left(x\left[\frac{1.75+x^2(1+\exp(-\zeta)^2)}{(1-x(1+\exp(-\zeta))}\right]^{1/2}\right) \qquad (2.6)$$

where.

$$\zeta=\frac{nF}{RT}(E_{appl}-E_0) \quad ; \quad X=i/i_{lim} \qquad (2.7)$$

The resulting plot is shown in Figure 2 7. After linear regression, the best fit line is $Y= ME_{appl}+B$ where M is the slope and B the intercept Matsuda has shown that (see reference 9, equations 44,45 and 49) the transfer coefficient α is related to the slope of the regression line (M) and several other known quantities by the expression

$$\alpha=M\frac{RT}{nF} \qquad (2.8)$$

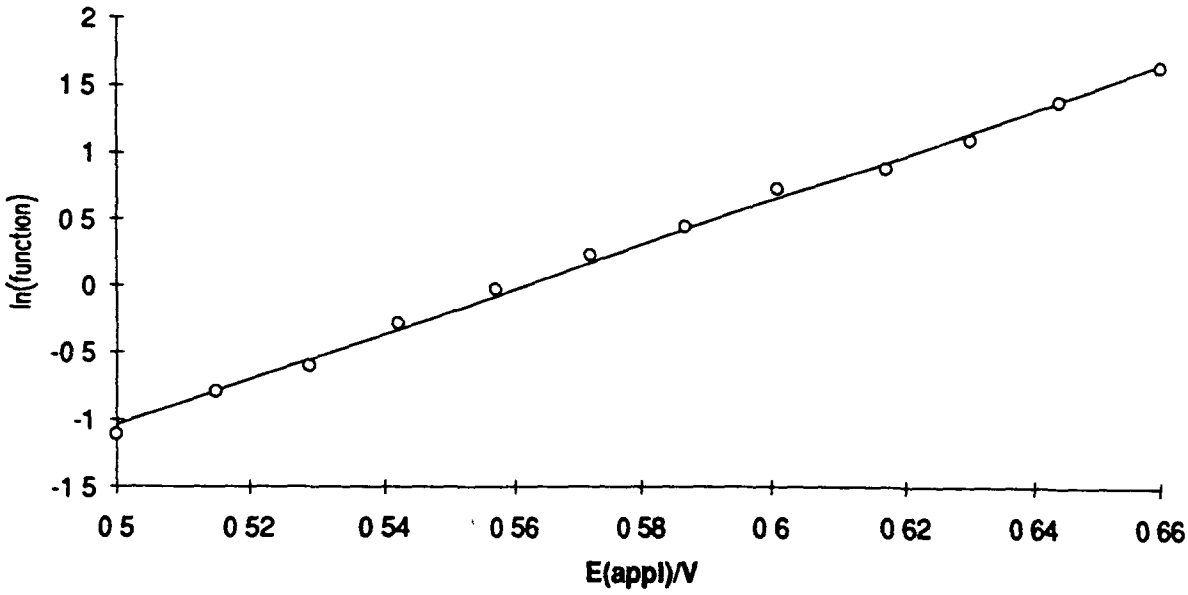

Figure 2.7. Best fit line obtained from the trace with 2 ms sampling time, as shown in Figure 2 6 after data transform (Equation 2.6). From the slope (M = 16.412) and intercept (B= -9.412) k_o and α can be evaluated (see below).

The heterogeneous rate constant k_o may be determined from (reference 9, equation 49)

$$\ln k_o + \ln\frac{4\sqrt{t}}{\sqrt{3D_{ct}}} = \ln\left(x\left[\frac{1.75+x^2(1+\exp(-\zeta)^2)}{(1-x(1+\exp(-\zeta))}\right]^{1/2}\right) \quad (2.9)$$

When $E_{appl} = E_o$ and with substitution and rearrangement we get·

$$k_0 = \frac{\sqrt{3D_{ct}}}{4\sqrt{t}} Exp\left[-(ME_0+B)\right] \quad (2.10)$$

which gives k_o in terms of known quantities. Hence values for k_o and α can be calculated for each of the sampling times employed.

2 5 Chronoamperometry

2.5.1. Description of the technique

This technique employs one large potential step (typical height 1 V starting 0.5 V below $E_{½}$) and the resulting transient is recorded again directly after the onset of the pulse Under assumption of a semi-infinite diffusion regime at the electrode during the rise of the pulse and ideal diffusional behaviour (only driving force for movement of ions is concentration dependant and not influenced by the presence of a strong local electric field, *i e* absence of migration) this transient should follow the Cottrell equation

$$i(t) = \frac{nFAC_o\sqrt{D_{ct}}}{\sqrt{\Pi t}} \qquad (2.11)$$

From a Cottrell plot (i vs $t^{-½}$) one may obtain a value for the homogeneous diffusion coefficient D_{ct} as outlined in the previous section

On comparing the D_{ct} values obtained by linear sweep voltammetry and chronoamperometry, the diffusion coefficient from the pulse experiment is usually one order of magnitude faster than the value obtained in the sweep experiments Although both types of experiments impose a semi-infinite diffusion regime upon the system, there is a difference If one uses a wider range of sweep rates (0 1 V/s -100 V/s) all of which impose a semi-infinite diffusion regime, not all of the i_p values will hold a linear relationship Apparently when sweep rates go above a certain rate there is a change in transfer mechanism The rise time of the pulse used in our set up is 20-30 μs for a 1 V step, which would correspond with a sweep rate in the order of 30 kV/s. On this alone it is clear that caution is necessary when comparing these two techniques During the pulse experiment there are definitely different mechanisms at work, perhaps in conjunction with the charge transfer occurring during the sweep experiment

2.5 2 Specifications and data acquisition software details

The software allows the user to change settings such as total number of pulses applied and pause duration in between pulses during data acquisition Also the program checks

whether the proper current range is selected as before The pulse train is generated by setting the DAC to the respective voltage level, while using the millisecond delay function of Turbo Pascal 6 0 to delay between pulses DMA (on the I/O board) is used to capture the traces which are then averaged (unity weight) if more than one trace is stored

2 5 3 Analysis software details

After entering the temperature, electrode diameter, number of electrons involved and the concentration of the active species, the i(t) data is averaged if there has been more than one pulse and plotted vs $t^{-½}$ and a time window can be selected over which the Cottrell equation (Eq 2 5) [8] will be evaluated By selectmg various windows the operator can evaluate D_{α} values for various time windows in a single run, which should lead to convergence

2 6 Brief description of Analog Devices RTI-815 I/O card.

2 6 1 General overview of functions present on the RTI-815 I/O board

The I/O card used as a hardware link between PC and electrochemical equipment employs two CMOS input multiplexers which provide analog input capacities for 16 single-ended inputs (or 8 differential inputs) The gain on these inputs is adjustable in software from 1, 10, 100 or 500 and the range is jumper selectable from 0-10 Volts, -5/+5or -10/+10Volts The analogue-to-digital conversion is handled by a 12-bit converter which can be configured to receive mputs in the 0-10, -5/+5or -10/+10 Volts range

The conversion resolution is 4096 counts (2^{12}) resulting in a 2 44 mv resolution in the first two ranges and 4.88 mv in the -10/+10 V window Analog-to-digital conversion times are 25 μs for a single channel at unity gain High speed data transfer is obtained employing the direct memory access (DMA) and interrupt circuitry of the board, which operates the DMA controller on the motherboard of the PC via an interrupt as soon as the data collection is finished Analog output features are provided by two 12-bit digital-to-analog converters, which can be set individually by jumpering in either 0-10 Volts or -10/+10 Volts range (output resolution 2 44 mV or 4.88 mV). These channels are capable of generating a 1 Volt step with a risetime of <30 μs.

2 6 2 RTI-815 I/O map and software control

The I/O mapping into the PC's I/O channel is laid out as depicted in Table 2.1 (next page) An x indicates a data-insensitive bit, and a z notates a zero-bit Finally, R/W stands for Read/Write and R (or W) for the respective single operation,S=scan-enable, G=Gain and M=Mux Installation and software control of the I/O card is relatively easy An unused base address located in the PC's I/O channel is selected (*e g* 320H) by jumpering and the board is plugged in one of the full-length expansion slots on the PC's motherboard Extensive control of the I/O card can be achieved using the drivers provided by Analog Devices, which can be accessed via a runtime user interface that hooks into assembly routines A separate DMA driver has to be loaded before one can make use of the parallel data processing facility

The following Pascal code in which assembly language is embedded may serve as illustration how these drivers possibly interact with the card (p 23)

Base+15	Unused	x	x	x	x	x	x	x	x
Base+14	Unused	x	x	x	x	x	x	x	x
Base+13	Control Status (R/W)	7	6	5	4	3	2	1	0
Base+12	Data (R/W)	7	6	5	4	3	2	1	0
Base+11	Digital O/P (R/W)	7	6	5	4	3	2	1	0
Base+10	Digital I/P (R/W)	7	6	5	4	3	2	1	0
Base+09	Flags Clear (W)	x	x	x	x	x	x	x	x
Base+08	DAC 1 High (W)	x	x	x	x	11	10	9	8
Base+07	DAC 1 Low (W)	7	6	5	4	3	2	1	0
Base+06	DAC 0 High (W)	x	x	x	x	11	10	9	8
Base+05	DAC 0 Low (W)	7	6	5	4	3	2	1	0
Base+04	ADC High (R)	z	z	z	z	11	10	9	8
Base+03	ADC Low (R)	7	6	5	4	3	2	1	0
Base+02	Convert Command (W)	x	x	x	x	x	x	x	x
Base+01	MUX/Gam (R/W)	S	G	G	M	M	M	M	
Base	Status (R)/ Control (W)								

Table 2.1. RTI-815 I/O Channel memory map.

The function ReadChannel reads a bit count (0-4095) from a specified channel with the requested software gain The function enforces the gain and channel on the multiplexer by writing a byte to the Base+1 address, as specified in the documentation supplied with the card This is followed by initiating the analog-to-digital conversion by writing to address Base+2, and looping until bit 6 in the status byte read from the base address has been set, indicative of the conversion being finished Finally a word (16 bits) is read from the Base+3/4 address of which the lowest 12 bits are significant and carry the bit count

```
Function ReadChannel( Chan·byte, Gain . Word )· Word,
Var
  rv :word;
  LABEL AGAIN;

begin
  Case Gain Of
    1   · Gain_Bit·=0; 10    . Gain_Bit·=32;
   100  : Gain_bit·=64, 500    Gain_Bit =96;
  else begin
    gain.=1,Gain_bit  =0,                    (* default Gain is 1 *)
  end;
end;
  asm
    MOV   AL,Gain_Bit            (* Gain bitmapped *)
    MOV   BL,Chan                (* Selected Channel *)
    OR    AL,BL
    MOV   DX,321H                (* Points to the Multiplexer (Base+1) *)
    OUT   DX,AL                  (* Sets Gain/Channel  on Mux          *)
    MOV   DX,322H                (* Starts Conversion (Base +2)  *)
    OUT   DX,AL
    MOV   DX,320H                (* Polls/Loops till Done *)
    AGAIN  IN   AL,DX            (* Reads  Status Byte    *)
    AND  AL,40H                  (* Bit 6 Status          *)
    JZ AGAIN                     (* End of the Loop       *)
    MOV   DX,323H                (* Reads Data Bytes    Base + 3/4  *)
    IN AX,DX
    MOV RV,AX
  end, (* asm *)
  ReadChannel =RV;
end,
```

2 7 Summary

The work described in this chapter has been carried out to implement a hybrid analog-digital system capable of measuring and analysing I/V characteristics of PME's in order to obtain parameters concerned with homogeneous and heterogeneous charge transfer across the electrode-film-electrolyte boundaries Objectives were the following a) easier operation of hardware due to partial software control and b) data retrieval, processmg and analysis on a digitised basis

References

1 a) R W Murray et al , Anal Chem , **59**,379-390,1987
b) R W Murray, Acc Chem Res ,**13**, 135-141, 1980

2 a) Inorganic Synthesis Series, Part 24
b) O Haas and J G Vos, J Electroanal Chem , **113**, p 139, 1980

3 Donal Leech, Ph D Thesis, Dublin City University, 1991 and references therein

4. A J Bard and L R Faulkner, Electrochemical Methods, Wiley, 1980, p 218

5 B D J R Fennema and G Hughes, First Annual Report of Science Grant # SC1000414, Dublin City University, 1991

6 A Savitsky and M.J E Golay, Anal Chem ,**36**, 1627, 1964

7 A J Bard and L R Faulkner, Electrochemical Methods, Wiley, New York, 1980, p 138

8 A J Bard and L R Faulkner, Electrochemical Methods, Wiley, New York, 1980, p 143

9 H Matsuda, Bull Chem Soc Jpn , **53**, 3439-3446, 1980

Chapter 3

Design and implementation of a data acquisition and analysis system to be used for impedance spectroscopy studies

3.1. Introduction to Impedance Spectroscopy

Impedance spectroscopy (IS) is a powerful non-destructive method of characterising electronic properties of a wide range of materials It may be used to investigate the dynamics of bound or mobile charge in the bulk or interfacial regions of any type of material, either in the solid or liquid phase [1].

The general approach is to apply an electrical stimulus (a known current or voltage) to the system under investigation and observe the response (a voltage or current respectively). Three different types of stimuli are used:

1) Transient impedance spectroscopy employs a step-function ($V(t)=V_0$ for $t>0$, $V(t)=0$ for $t<0$) to disturb the system and the resulting current transient is captured and analysed This yields the ratio $V_0/I(t)$ (so-called indicial impedance or time-varying resistance) Although an easily accessible quantity experimentally, this is usually Fourier-transformed from a response-time domain into the response-frequency domain for analysis and interpretation of the data Experimentally this type of modulation is easily achieved and a digitising storage oscilloscope or I/O card could be used to capture the trace, disadvantages being the need to carry out a FT and the frequency range is dictated indirectly (via the step function) and therefore not all desirable frequencies may be covered

2) Another method is to apply a truly random white noise signal V(t) to the sample followed by FT analysis of the resulting i(t) response The advantage of this particular technique is that submitting the cell to a white noise stimulus results in a current response carrying a broad frequency range Disadvantages are the technical difficulties in obtaining true white noise and a limit in frequencies which are covered by this technique (50 Hz-100 kHz) using digital-to-analogue electronics and Fourier transform algorithms are difficult to implement for frequencies below 10 Hz

3) The last technique is technically the most feasible one by measuring directly in the frequency domain, thereby cutting out the need for FT processing This is done by applying a single-frequency voltage to the system and measuring the resulting phase shift and amplitude of the current (or real and imaginary parts) at this particular frequency. The frequency range spans up to nine decades (1 mHz-1 MHz) The technique is relatively uncomplicated, and calculations involved are straightforward. However due to the fact that one can only measure one frequency at the one time the method is time consuming

A few assumptions are usually made in impedance spectroscopy studies·

a) The system is in a steady state, i e the properties are time invariant
b) The modulation is sufficiently small as to allow the system to maintain an equilibrium state, at least in close approximation
c) The system should display a linear response towards the disturbance caused by the modulation (i e applying 2*|V| should result in twice as high a current response). The models and equations used for impedance analysis only hold in this linear region and therefore this should be checked for the specific system Usually one employs signals which amplitude is smaller than the thermal voltage (V_T =RT/F=kT/e, ≈25 mV at 25 °C, as outlined in reference 1)

3 2 Response to a small amplitude stimulus in the frequency domain

In this section the basic mathematics involved in IS will be introduced [1]
A single frequency signal $v(t) = V_o Sin(\omega t)$ (with $\omega = f/2\pi$) is applied to system and the resulting steady state current $i(t) = I_o Sin(\omega t+\Theta)$ is measured Θ is the phase shift arising from capacitive behaviour within the system (Θ=0 for purely resistive characteristics)

The conventional impedance $Z(\omega)$ is defined by $v(t)/i(t)$, with modulus $|Z(\omega)| = V_o/I_o(\omega)$ and phase angle $\Theta(\omega)$ Impedance can be represented as a complex quantity $Z = Z' + jZ''$ ($j=\sqrt{-1}$) in which Z' is the resistive part and Z'' the reactive contribution to the overall impedance Z, or the in-phase and 90° out-of-phase components respectively The reactance is responsible for phase shifts and is linked to capacitance through $Z'' = 1/\omega C$

$Z(\omega)$ can be plotted in the complex plane as depicted in Figure 3.1 and the following quantities can be derived from this.

$$Im(Z) = Z'' = |Z| \, Sin(\theta) \tag{3.1}$$

and the phase angle is given by

$$\theta = Tan^{-1}(Z''/Z') \tag{3.2}$$

and the modulus of Z·

$$|Z| = \sqrt{(Z')^2 + (Z'')^2} \tag{3.3}$$

This defines the Argand diagram (Figure 3.1, overleaf) and in polar coordinates the impedance can be written as $Z(\omega) = |Z|\exp(j\Theta)$ and using Euler's rule this becomes $Z(\omega) = |Z|\{\cos(\Theta) + j\sin(\Theta)\}$.

Note that this quantity has become time-independent as expected for a steady state technique (and only if the system is time-invariant as well).

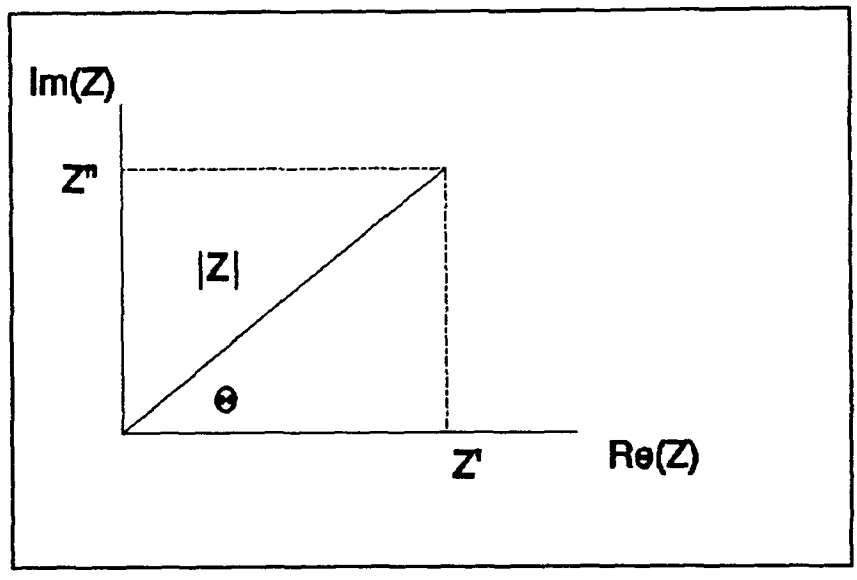

Figure 3.1. Argand diagram showing the various quantities related to the impedance Z in the complex plane

3 3 The single frequency impedance measurement technique.

We favoured the single-frequency approach (as described in 3 1) over the transient or white noise method because of its technical simplicity The basic experiment is based on measuring the transfer function of the system. This function describes the inverse ratio in which the input signal is transferred into the output signal depending on the angular frequency used and can be given as.

$$G(j\omega) = X_{out}(j\omega) / X_{inp}(j\omega) \qquad (3.4)$$

In the special case where X_{inp} is a modulation current and X_{out} is the resulting steady-state voltage, G(jω) is equal to the impedance of the system

$$G(j\omega) = V(j\omega) / I(j\omega) = Z(j\omega) \qquad (3.5)$$

The impedance will be a complex quantity ($Z = Z' + jZ''$) in order to accommodate for a possible change in two parameters, phase and amplitude, as a scalar quantity is capable of conveying only over one changing parameter

The experimental setup for this so-called direct measurement consists of the following minimum components [a]

1) modulation source (sine wave generator)
2) phase sensitive detection (oscilloscope or lock-in amplifier)

The technique is called direct method because it acts directly in the frequency domain, whereas transient and white noise methods are performed in the time domain and have to be transferred into the frequency domain by Fourier transform The phase sensitive detection used in the instrumental setup described in this thesis is a lock-in amplifier This yields the following advantages over a oscilloscope as means of detection·

a) Because of the need for small modulation signals (in order to stay within the linear response range of the system) response signals are usually small and will need amplification This in combination with the fact that IS, as other AC-based measurements, tends to be noise prone (AC pick-up) makes a lock-in amplifier (LIA) a good detection technique

b) Determining the impedance parameters from oscilloscope data is done by visible inspection of the data on the screen (or hard copy) This makes automatisation of the technique very difficult In contrast, most modern LIA's are equipped with RS-232 and/or IEEE-488 (GPIB) interface connectors in order to facilitate interfacing

[a] Our specific setup is described in detail in Section 3.4

From Ohm's law (V=IZ) it follows directly that

$$Z=\frac{V'+jV''}{I'+jI''} \tag{3.6}$$

Phase sensitive detection may be achieved by operating a multiplexing and time-averaging circuit sequentially. The multiplexer effectively multiplies the input sine wave V_i with a reference square wave V_{ref} Written in Fourier components V_{ref} looks like.

$$V_{ref}=(4/\pi)\{\sin(\omega_r t)+\tfrac{1}{3}\sin(3\omega_r t)+(1/5)\sin(5\omega_r t)+\quad\} \tag{3.7}$$

and the input sine wave V_i can be written as $V_i:=|V_o|\sin(\omega_i t+\Theta)$ where V_o is the modulation amplitude and ω the angular frequency of reference (subscript r) and input (subscript i) respectively This will result in the following multiplexer output:

$$\begin{aligned} V_{mpx}=V_{ref}*V_i=\ & (2|V_o|/\pi)*\{\cos([\omega_i-\omega_r]t+\Theta)+ \\ & \tfrac{1}{3}\cos([\omega_i-3\omega_r]t+\Theta)-\tfrac{1}{3}\cos([\omega_i+3\omega_r]t+\Theta)+\ .\ \} \end{aligned} \tag{3.8}$$

Normally ω_r and ω_i are identical (i.e same source) and therefore V_{mpx} simplifies towards.

$$\begin{aligned} V_{mpx}=\ & (2|V_o|/\pi)*\{\cos(\Theta)+ \\ & \tfrac{1}{3}\cos(-2\omega t+\Theta)-\tfrac{1}{3}\cos(4\omega t+\Theta)+\quad\} \end{aligned} \tag{3.9}$$

Note that only the first term is time-independent and will therefore survive the time-averaging circuitry (all following terms go to zero on averaging)

$$V_{mpx}=(2|V_o|/\pi)*\cos(\Theta) \tag{3.10}$$

This is a phase sensitive DC output voltage (depends on the cosine), which is maximised at $\Theta=0$ The detector's output has to be frequency selective, apart from being phase-sensitive This is another feature of equation 9 the time-average over this equation for ω_r unequal to ω_1 is zero, apart from odd-order harmonics of the input signal (n.=3,5, ..). This does not really present a problem since the contribution of the 'overtones' diminishes with order if a square wave reference signal is used (generated internally by the LIA). The LIA used in this study employs a sinusoidal reference signal and in this case the odd-harmonic overtones are much smaller.

3.4 Setup Hardware

The instrumental setup consists of a Stanford Research SR-510 Lock-in amplifier combined with a function generator, PC-AT compatible PC, and some in-house manufactured electronics, which features will be described below. A schematic diagram is given in Figure 3.2. The switch-selector S (see 3.8 for details) is used in order to allow the single channel SR-510 to measure the V and I signal lines sequentially under PC control The summing junction SJ (3.8) was build to minimize the existing impedance difference between the function generator and the DAC (back-panel LIA) used, which allows the bias across the sample to be set under software control The current-to-voltage transducer circuit CTV operates at a gain of 5.110 K (3 8) Sample probes are spring loaded and all cabling outside the metal box is coaxial cable connected to floating BNC connectors All electronics are grounded at mains-ground on the power supply

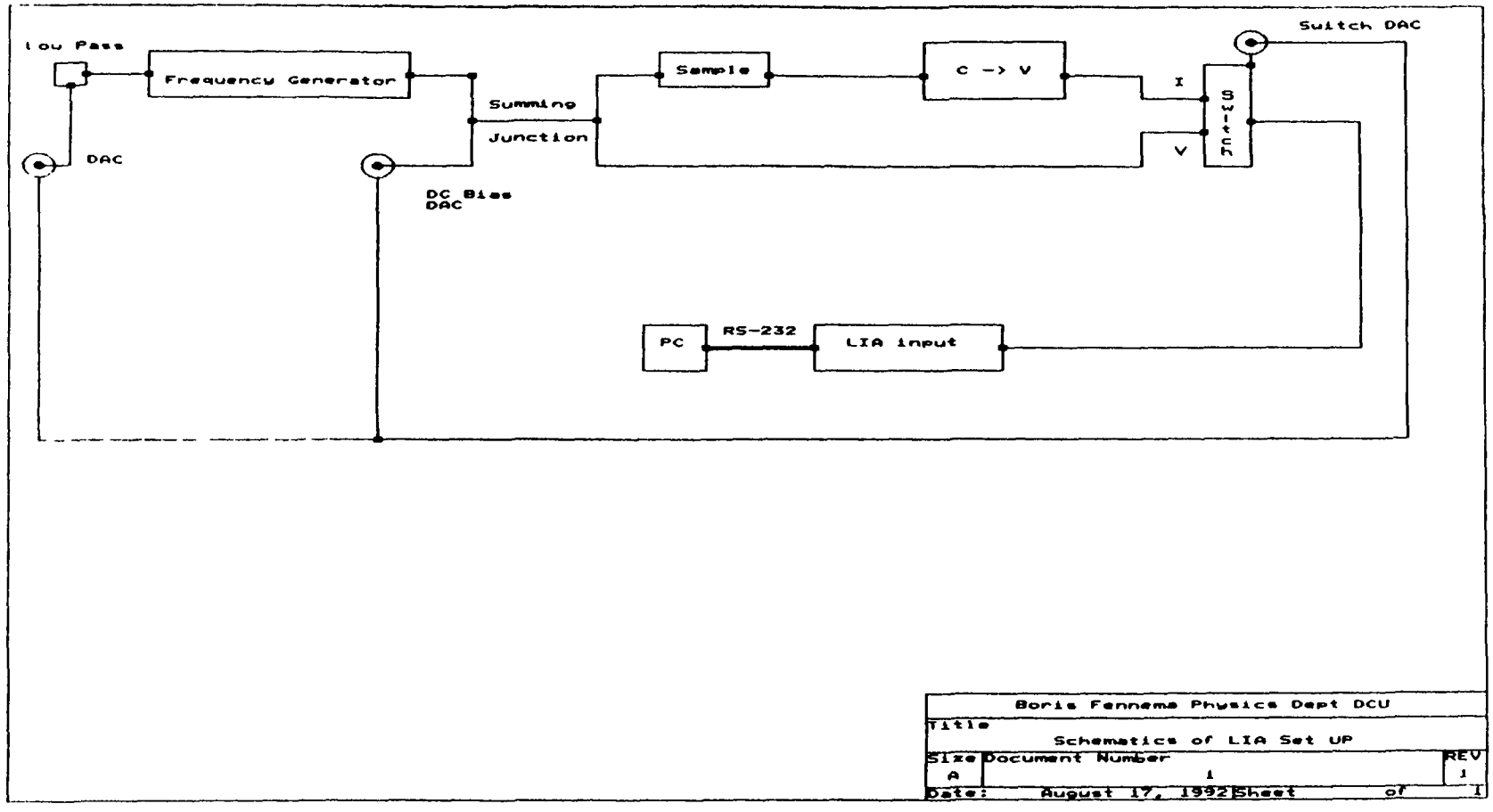

Figure 3.2. Schematic diagram of the hardware setup used The LIA controls bias and switch through 2 DAC's located on the rear-panel of the SR-510 The frequency is swept using a DAC (Bytronic) which is placed in one of the free expansion slots located on the PC's motherboard

3 5 Software details

3 5 1 Specification

Due to the fact that measurement times tend to be long (up to approximately 30 seconds a point, depending on the value of the time constant set on the LIA) the software has to be capable of controlling the flow of the experiment without assistance of the operator. The program can be expected to run overnight or over long periods and this has consequences for the design of the program. The program can be run in a test mode in which frequency and switching is done manually to enable the operator to check the correct functioning of the equipment, but will usually be run in an automatic mode Therefore the program has to be robust, *i.e.* it has to be protected against infinite loops and error handling has to be implemented around calculations, disk I/O and memory allocations Parameters such as frequency and bias ranges are set using two menus and stored on disk. A simple plotting facility is included, incorporating an overlay procedure The quality of the plots is too low for publication purposes and therefore there is the possibility of exporting data in an ASCII format, with a choice of delimiters, in order to ensure compatibility with a wide range of commercial DTP packages and spreadsheets. A flow chart of the data acquisition routine is presented in Figure 3.3.

3 5 2 Data acquisition details

The program calculates the resistance and capacitance as outlined above using Eq 3 7 Firstly, the phase is optimised and set to 45 degrees in order to avoid the situation of dividing two numbers which are of very different magnitude, which would result in a large error. For the first point of a bias sweep at a certain frequency V' and V" are measured and these values are then successively used for all calculations in this sweep After measurement of V' and V", I' and I" are measured and the resistance and reactance calculated and displayed. All points are at least measured twice (maximum of 5) and the operator is informed if the data spreads around the mean by more than a previously set threshold (usually ± 5%) and data is stored in binary format after each sweep is completed

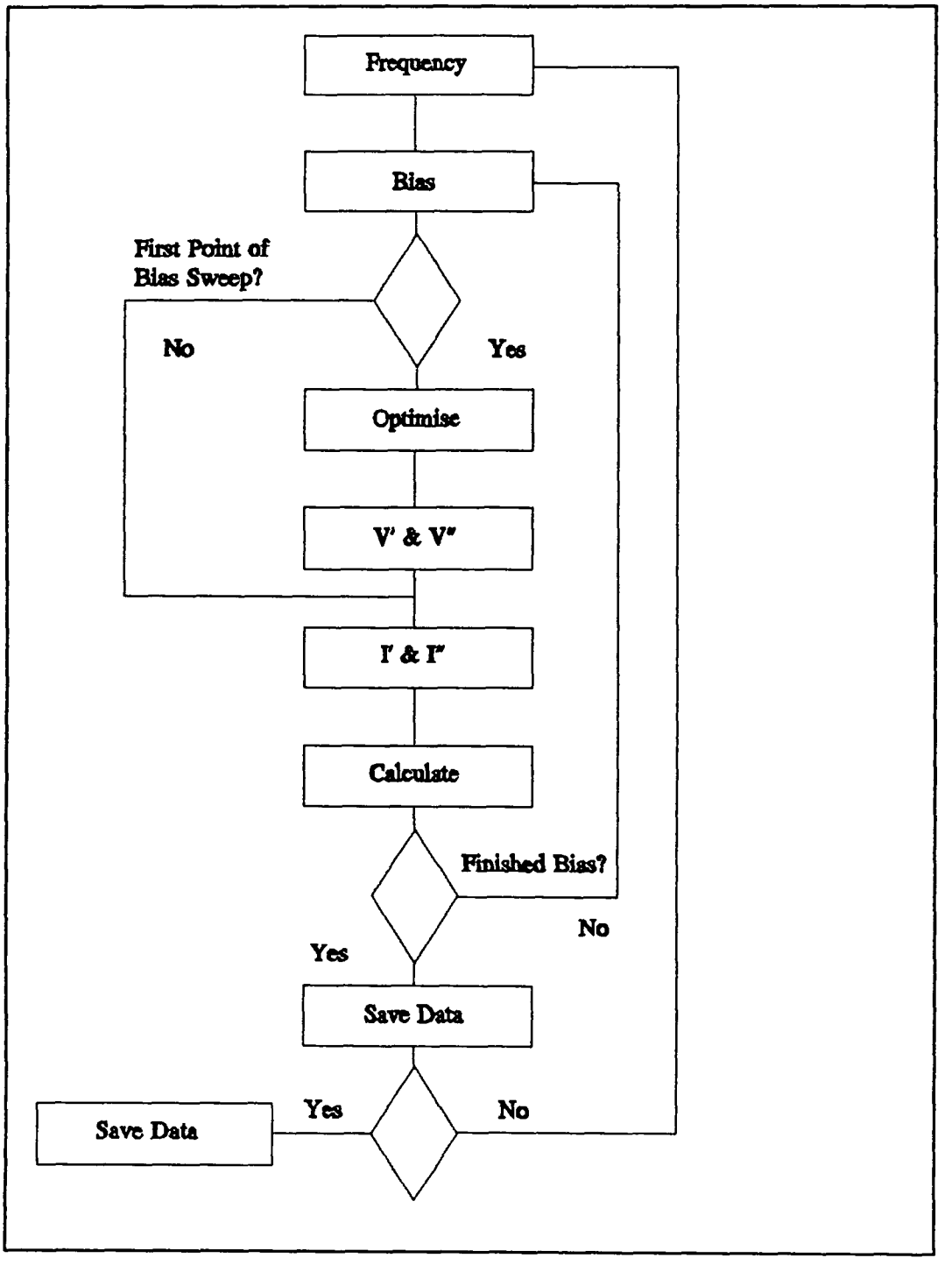

Figure 3.3. Flow chart of data acquisition routine The data is saved after each bias sweep or after each frequency sweep if the bias is maintained at one specific bias

3 5 3 Post Run Analysis

This consists of three plotting facilities to inspect the collected data on-screen combined with a routine that carries out a Mott-Schottky calculation based on equation (3 11)

$$\frac{1}{C^2}=\left(\frac{2}{\epsilon_o\epsilon_r n_d e}\right)(V-V_{fb}) \qquad (3.11)$$

Usually this expression contains a kT/q term (equal to 26 mV at 25°) which has been neglected This is due to the fact that the technique used in this chapter is capable of determining the flatband potential within ± 0 05 V and therefore does not allow for evaluation of kT/q, which has a magnitude smaller than the error margin [2].
Available plots are resistance vs bias, capacitance vs bias and $1/C^2$ vs applied bias These routines have been implemented to enable the operator to inspect the data directly after collection for verification purposes

Due to the fact that the data can be exported in an ASCII format, all additional calculations can be carried out using specialised application software or spread sheet packages, if necessary and also this provides a gateway towards high quality plots

3 5 4 Error Handling

The error handling used is based partly on an idea by Michael Tischer [3] and works by storing the CPU registers and the stack house keeping pointers before carrying out a potentially dangerous operation (calculation, disk I/O) This provides the program with a re-entry point if a run-time error is generated. In Figure 3 4 a flow chart displays the idea of error handling used Assume the program being in the middle of a procedure about to read something from disk or to divide two numbers. Just before the operation is carried out the contents of the stack and CPU registers are stored in a global buffer, the error flag is cleared and the jump flag is being set The program continues and carries out the operation If there is no run-error generated the program will continue, otherwise the error flag will be set and the exit/shutdown procedure called

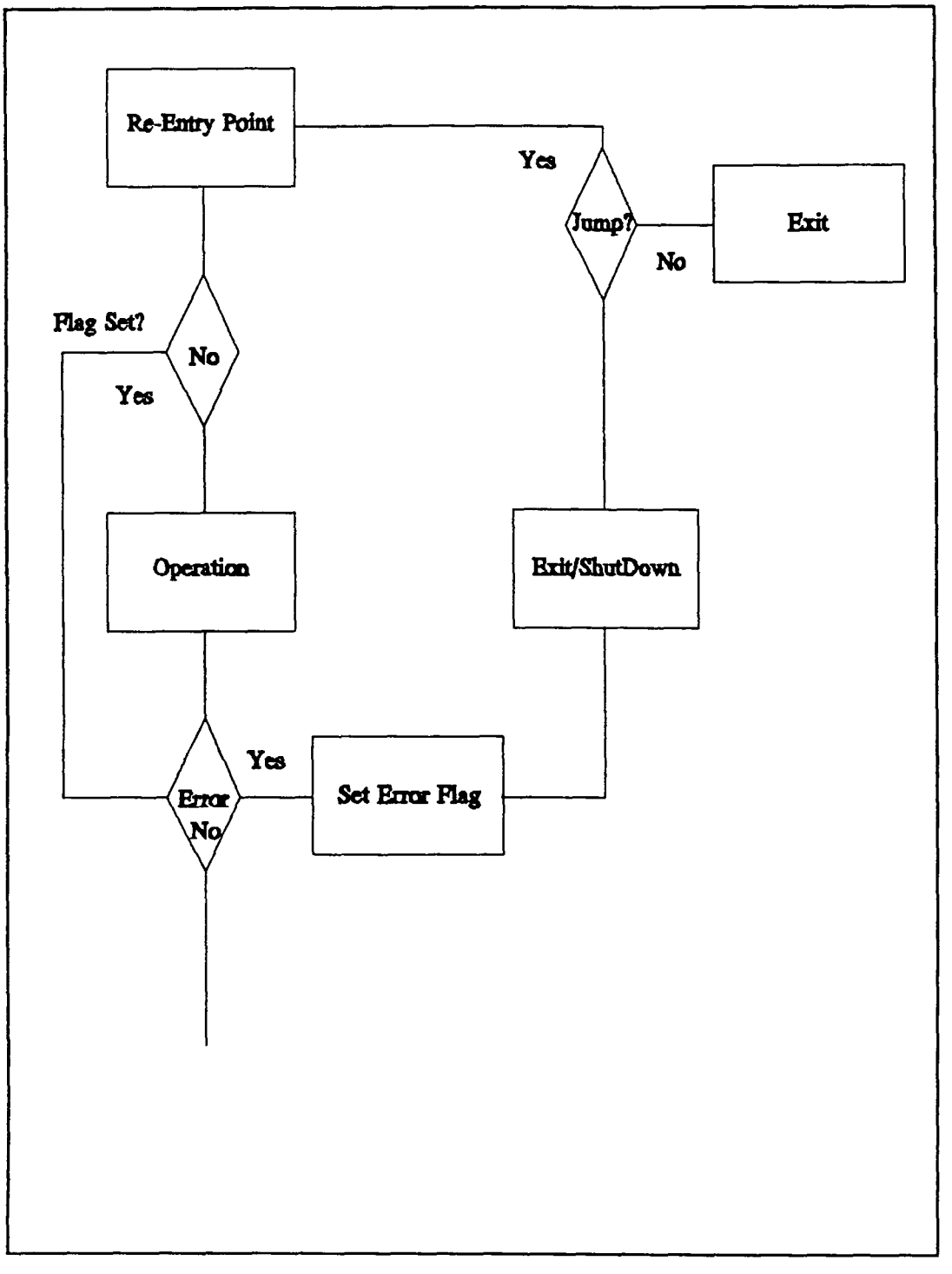

Figure 3.4. Error handler flow chart illustrating the concepts involved The two important features are the stack and CPU restoration needed for a successful jump to the re-entry point (see text for more details).

This procedure is a standard Turbo Pascal procedure which will be called on normal or forced program termination When the program has been forced to terminate by a run-time error **and** if there is a jump-location available, only in that instance will execution be re-started at the re-entry point, but now the error flag is set and the failed operation will be bypassed This system may look complicated but it results in a very general run-time error handler, which because it links into the default shutdown procedure (ExitProc [4]) within Turbo Pascal is very flexible and reliable

3 6 Validation and calibration of the system

The system has been calibrated against a Boonton capacitance bridge using a Motorola MV1404 tuning diode and an in-house manufactured MOS capacitor The tuning diode has been chosen for two main reasons, namely exhibiting a ten-fold decrease in capacitance over a 10 Volts reverse bias range combined with being frequency independent The diode was placed in the sample holder in series with a 100 Ohms resistor to limit the current flow Results are shown in Figure 3 5 and 3 6 From the graphs it is evident that the system is capable of measuring capacitance over a large frequency and bias range and as such can be used as a complementary tool of the Boonton bridge The advantage of this system is that the operator can choose the operatmg frequency, while the Boonton is fixed at 1 MHz In order to exploit this, it was decided to measure an in-house manufactured metal-oxide-semiconductor capacitor (MOS) This type of device is known to exhibit a high- and low-frequency limit in the capacitance profile [5] Therefore it was decided to exploit the variable frequency capacity of the instrumentation described in this chapter and try to establish these two limits

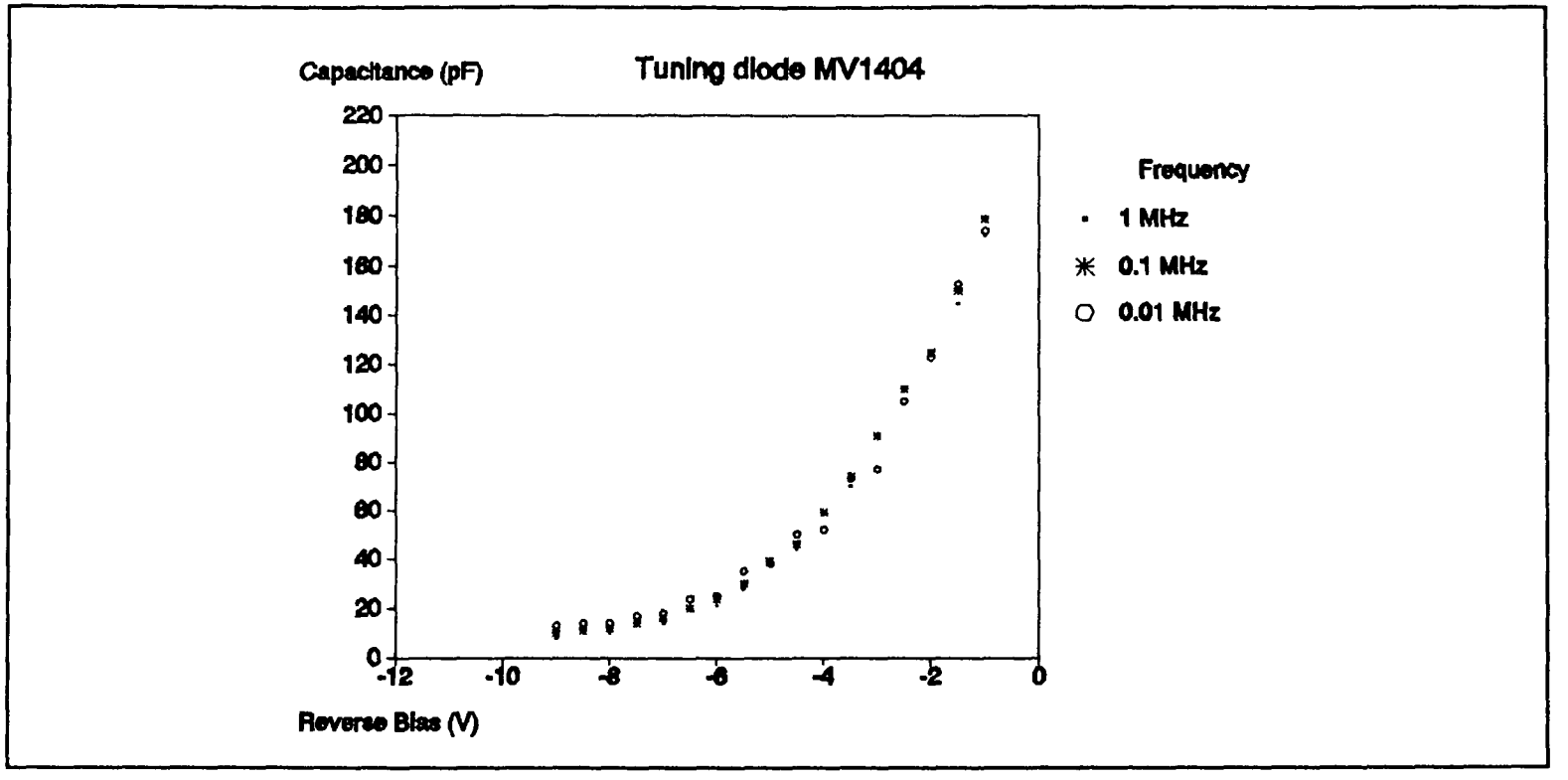

Figure 3.5. Plot of capacitance versus reverse bias of tuning diode MV1404 as measured on our system and the Boonton (1 MHz trace) Please note the very small change in capacitance over two order of magnitude in frequency at a particular bias Typical difference between Boonton values and LIA in the order of 1-2 pF. Modulation amplitude used < 25mV peak-peak Data is compiled from a minimum of three runs.

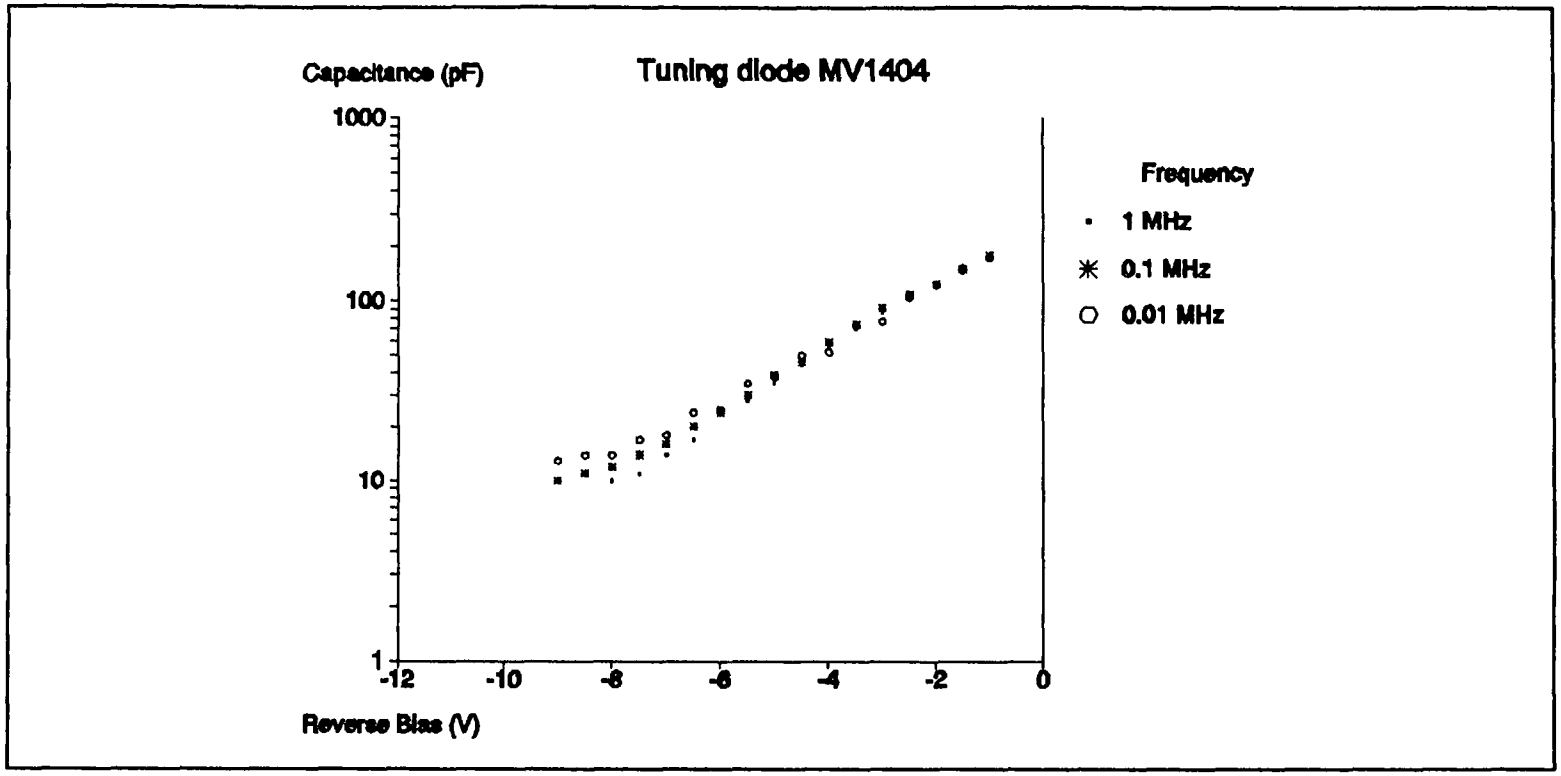

Figure 3.6. Plot of Log(Capacitance) versus reverse bias voltage The data from Figure 3.5 has been used in this plot Modulation amplitude used < 25mV peak-peak

Samples consisted of MOS capacitors based on aluminium oxide on silicon.
Data is depicted in Figure 3 7 while the effect of scan direction is shown in Figure 3 8 (p 42 and 43) This shows excellent performance of the system for frequencies above or round 1 kHz, below this the signal becomes very noisy and yields unreliable results. As can be seen from this figure, the overall capacitance of the MOS capacitor is dependent on bias, displaying distinct extremes in reverse and forward bias The overall capacitance is governed by the series capacitance of the metal oxide and the semiconductor, as given by Equation 3.12.

$$\frac{1}{C_{total}} = \frac{1}{C_{ox}} + \frac{1}{C_{semi}} \tag{3.12}$$

In forward bias, an accumulation layer is formed and C_{semi} reaches a minimum value, resulting in a maximum in the overall capacitance. Under reverse bias, a depletion layer is formed and C_{semi} goes through a maximum causing C_{total} to decrease. C_{ox} can be treated as constant. From this data, an estimated oxide layer thickness of 700 Å can be evaluated using Equation 3.13

$$t = \frac{\varepsilon_{ox}\varepsilon_{o}A}{C_{ox}} \tag{3.13}$$

in which ε_{ox} is the dielectric constant of silicon oxide (0 34 pF/cm [5]) and C_{ox} is the plateau value of the capacitance obtained under forward bias (3000 pF) and A the area of the MOS capacitor ($\pi(0\ 45)^2$ cm^2) Figure 3 7 and 3 8 clearly show a typical high frequency capacitance response of the MOS structure [5] Unfortunately, noise levels increased at the frequencies below 1 kHz, resulting in poor quality data Therefore, we have been unable to observe any typical low frequency behaviour

3 7 Summary and Conclusions

The system as presented in this chapter is capable of measuring capacitance with a degree of accuracy comparable to the commercial Boonton bridge. A drawback is the relatively long data acquisition times, but the fact that the operating frequency is user selectable from a 1 kHz-100 kHz window is a possible advantage of this system (below 1 kHz the data acquisition becomes very noisy) combined with a completely automated design of the experiment makes the system an attractive one to use

3 8 Electronics schematics and details

This section is included to give a brief schematic overview of the electronics used in the experimental setup as shown in Figure 3 2 More details can be found in the Appendix (including a list of materials used and connections) and in Jones [6]

The following four main components are used in the instrumentation a summing junction, a current-to-voltage transducer, a channel switcher and a low pass filter Schematics of the first three can be found in Figure 3 8, the latter is presented in Figure 3 9 The inverting summing junction is used to sum the AC modulation and the DC bias before the combined signal is passed on to the sample Note that in order to apply a particular bias to the sample an inverted (=oppositesign) signal must be fed into the DC bias input of the junction The resulting current response is sensed by the inverting current-to-voltage transducer and converted in a scaled voltage The fact that this transducer also inverts the signal has no effect on the calculations (all calculations exhibit a periodicity of 180°) Finally the two signals (modulation and response) are fed into the channel switcher

The low pass filter is merely used to remove any digital noise originating from the DAC that drives the frequency generator when the program is run in automated mode Any fluctuation in driver DC level would cause the frequency to drift, which in turn would render the obtained data useless Passing the DC offset through a low pass filter prevents this from happening

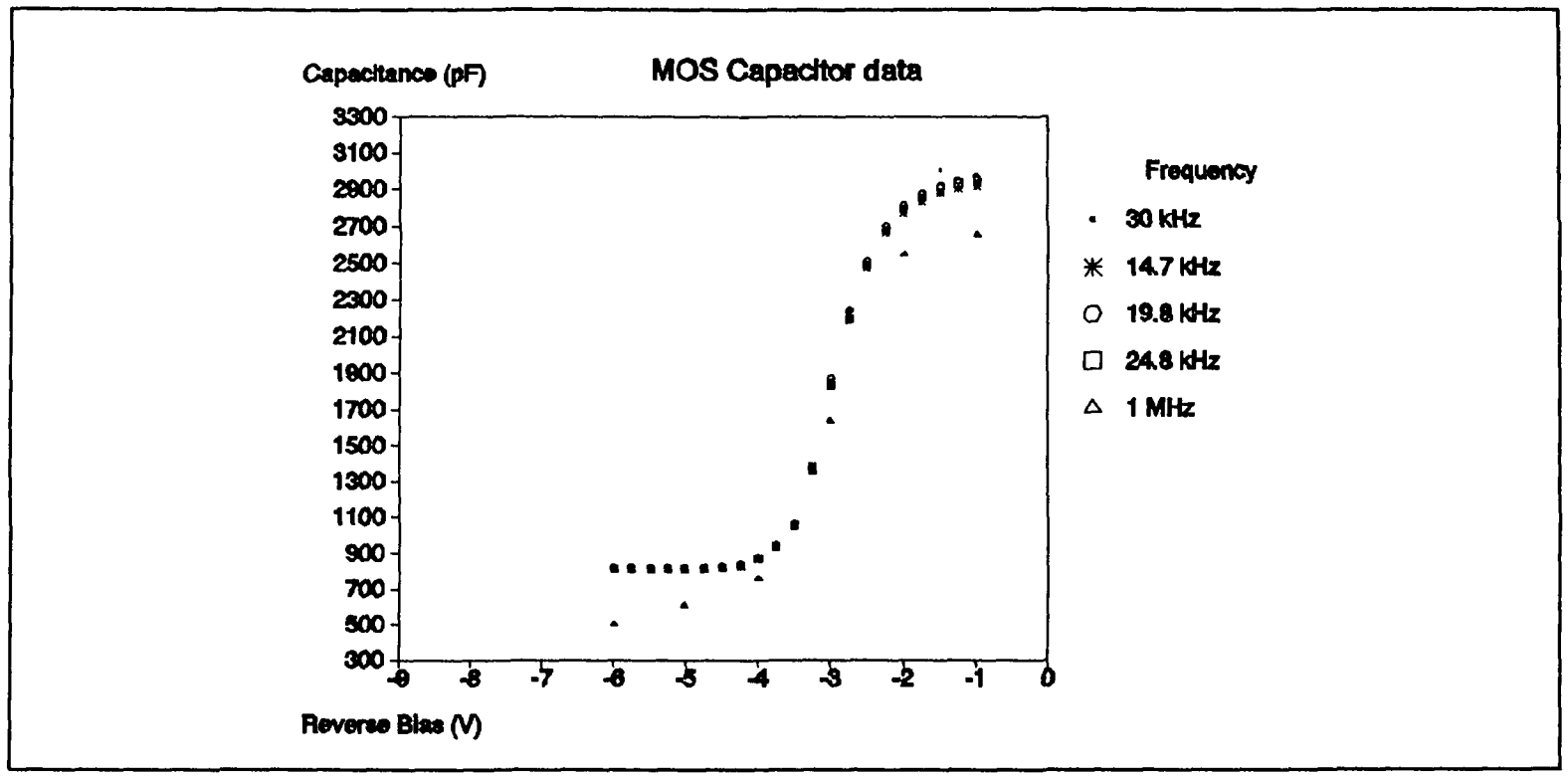

Figure 3.7. Capacitance data obtained on an in-house fabricated MOS capacitor The data has been measured using frequencies between 30 and 14 kHz and appears to be consistent For comparison reasons the figures obtained on the Boonton capacitance bridge are shown (1 MHz) Modulation amplitude used 30 mV peak-peak.

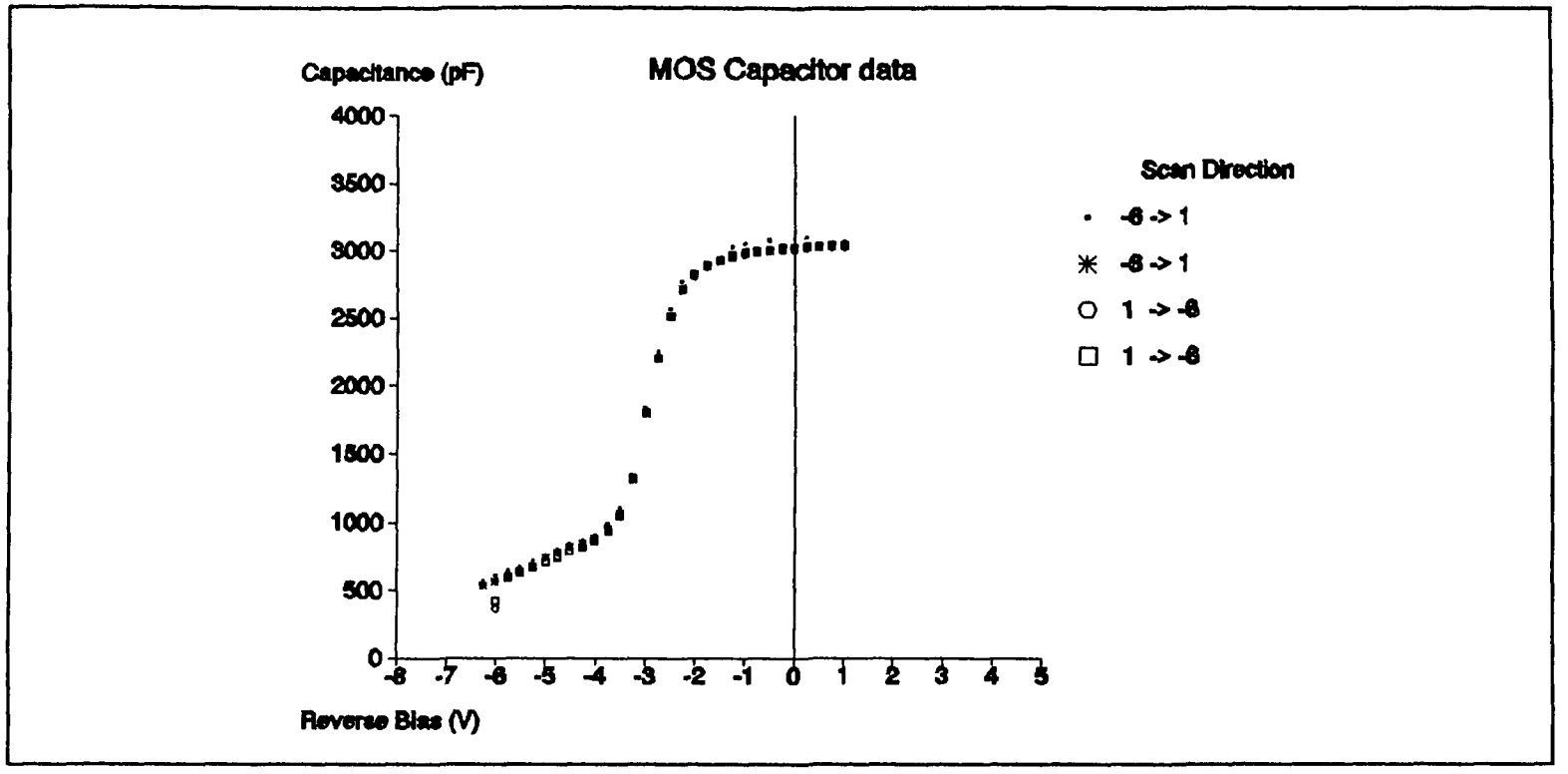

Figure 3.8. The effect of the direction of the bias sweep has been investigated Data is obtained at 59 kHz employing a sine wave with a 30 mV peak-peak amplitude

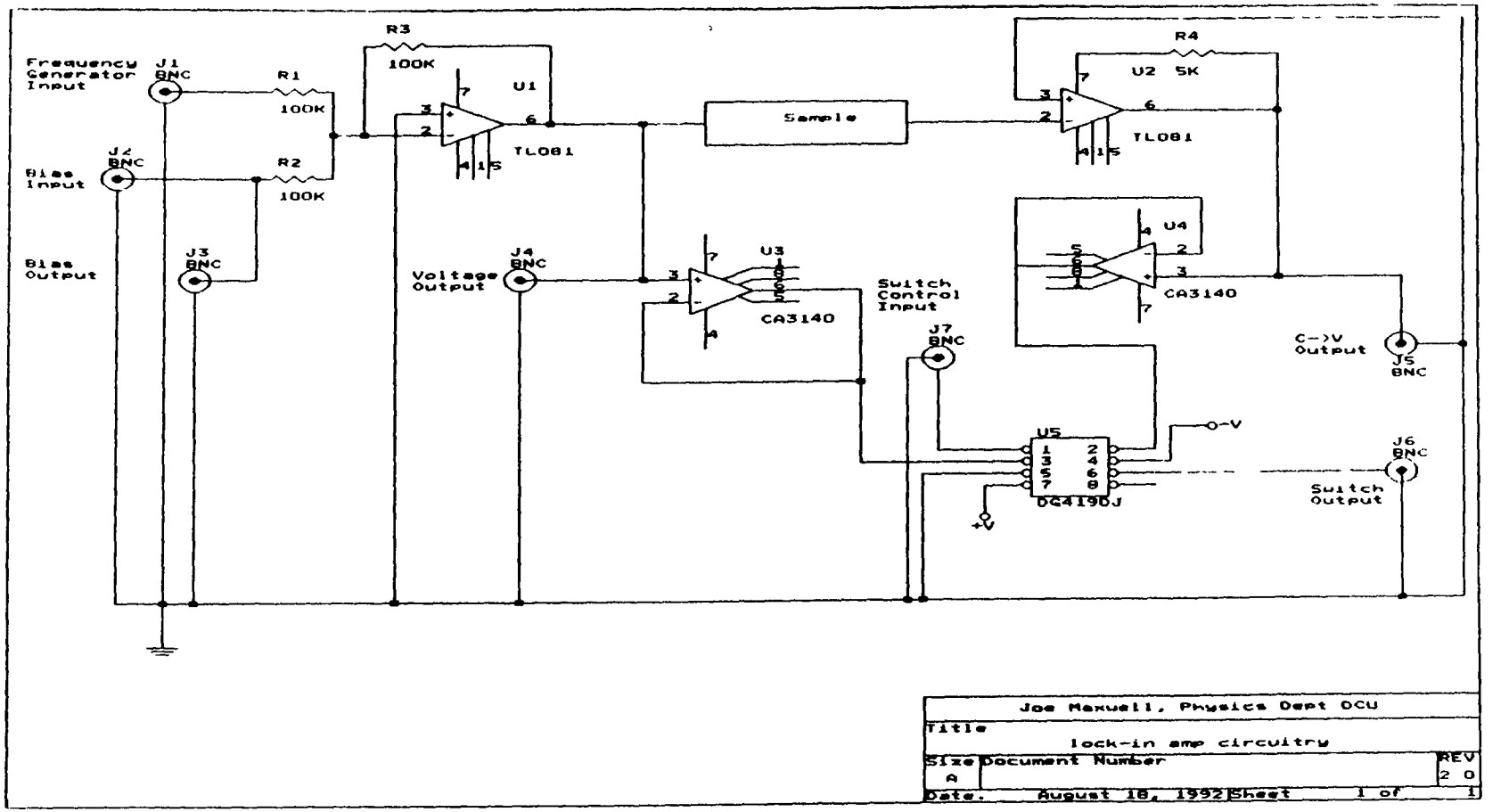

Figure 3.9. Schematic representation of summing junction, current-to-voltage transducer and channel switcher as employed in the experimental setup shown in Figure 3.2

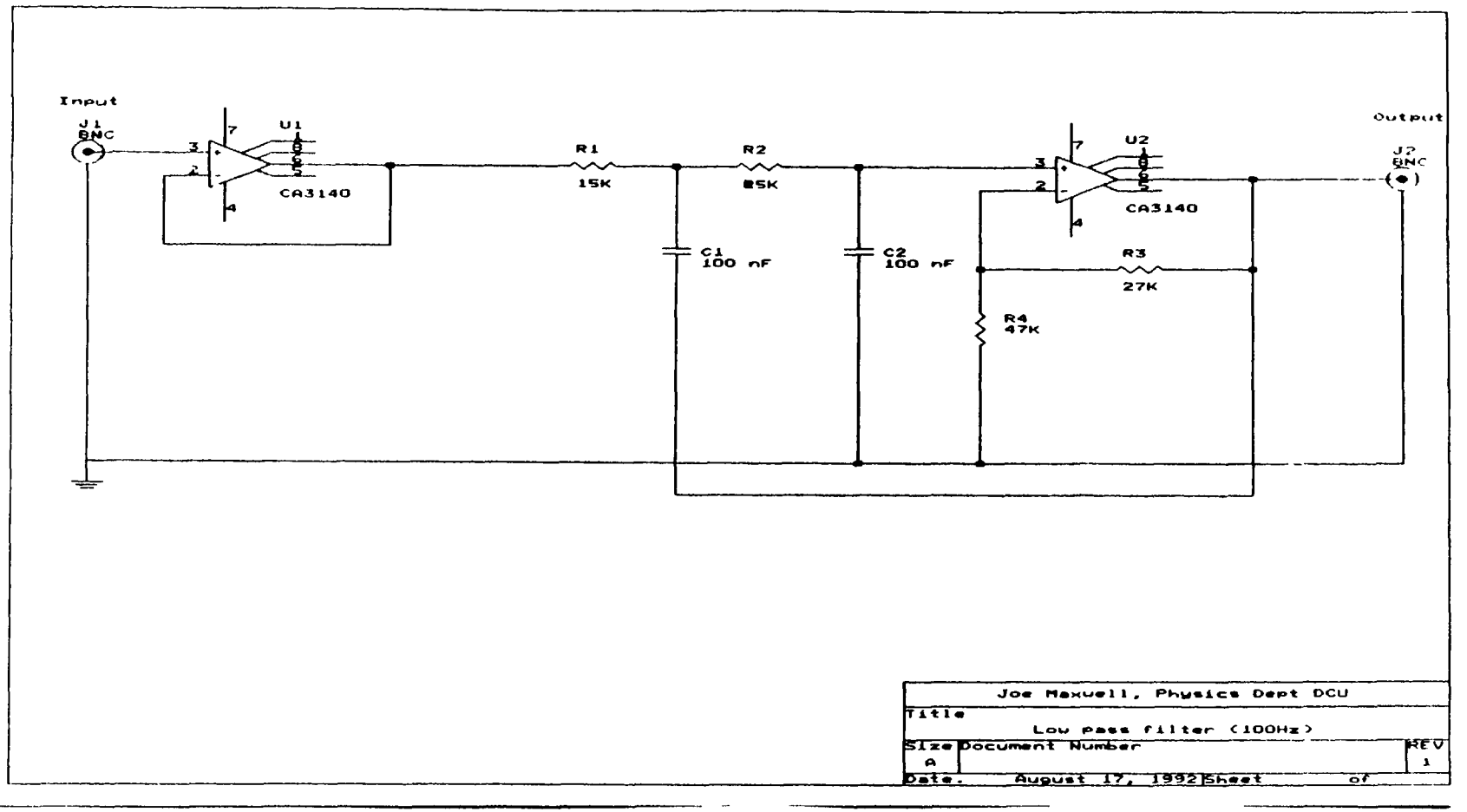

Figure 3.10. Schematics of low pass filter (cut off frequency 100 Hz) used to stabilise the DAC output originating from the Bytronic I/O board.

References

1 J R MacDonald (editor), Impedance Spectroscopy, Wiley, New York, 1987

2 H.O. Finklea (editor), Semiconductor Electrodes, Elsevier, 1988

3 M Tischer, Turbo Pascal Internals, Abacus, Grand Rapids, 1990

4 Turbo Pascal 6 0 Programmers Guide, Borland International, p 248, 1990

5. E.H. Nicollian and J R Brews, MOS (Metal Oxide Conductor) Physics and Technology, Wiley, 1982

6. M.H Jones, A Practical Introduction To Electronic Circuits, Cambridge, 1977

Chapter 4

Examples of Impedance Spectroscopy

4 1 Introduction

In this chapter capacitance measurements obtained on a gold coated gallium arsenide Schottky diode (Au-GaAs) using the setup described in Chapter 3 will be presented The reason for submitting the diodes to reverse and forward bias is to establish whether the instrumentation is capable of measuring capacitances accurately at both low and high current densities In reverse bias the diode will block the current and the resultmg current will only involve the leakage current In forward bias however the diode will allow current to flow and its resistance will drop with increasing forward bias which results in relatively high current densities The next section will explain in detail what the consequences are for the measurement technique The last section will deal with results on the diodes obtained at various temperatures.

4 2. Current density and its consequences on the technique

In the capacitance measurement as described in Section 3 5 2 using Equation 3 7 In brief, the calculation is based on the measurement of two values which are 90° out of phase with each other for both the current response and the voltage modulation The relative phase of the measurement is shown in Figure 4 1 (next page) The impedance is calculated by dividing the two complex numbers (Equation 4 1)

$$Z=\frac{V'+jV''}{I'+jI''} \qquad (4.1)$$

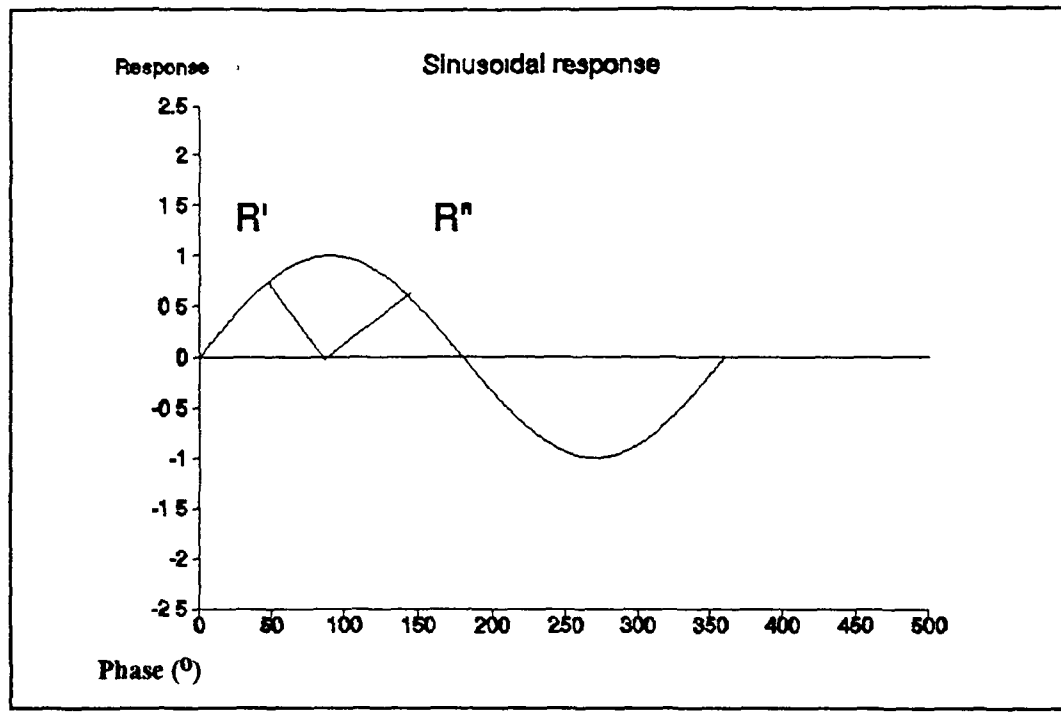

Figure 4.1. The relative orientation for the two data points R' and R" The points are 90° out of phase For the voltage modulation R = V,for the current response R = I

The measurement of the two orthogonal points characterises the respective sigmoidal signals (current and voltage) as explained in Section 3 2 regardless of applied bias. But at high current densities corresponding to forward bias there is a complication The problem does not arise with the characterisation of the sine wave but with the deconvolution of the output of the current-to-voltage transducer The current response is composed of a current originating from the resistive (or real) part of the impedance and a capacitive (reactance, imaginary) contribution These two components generate the actual current response as shown in Figure 4 2 (next page) with the resistive contribution being in phase with the voltage modulation.

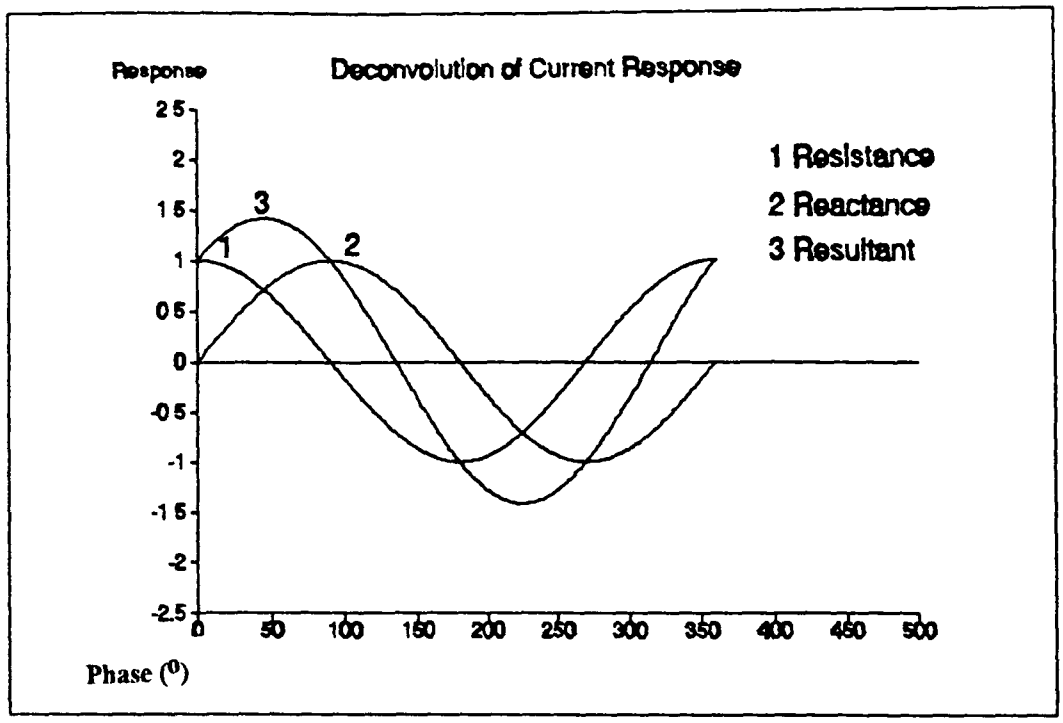

Figure 4.2. Deconvolution of the current response in terms of the two orthogonal contributions, resistance and reactance Note· the resulting shape contains information concerning both components. For clarity both amplitudes are set equal

The current response obtained if a Schottky diode is being measured under reverse bias is similar to that depicted in Figure 4.2 In reverse bias, the resistive contribution is only due to leakage current and therefore relatively small. In this case all four values in Equation 4 1 are of similar order of magnitude and hence the signal deconvolutes quite well However, in forward bias the current density is increased significantly compared to reverse bias and this results in current response more like the one displayed in Figure 4.3 (next page). In this case deconvolution using the technique described above will not work very well and the capacitance values obtained will not be a true representation of the capacitive component

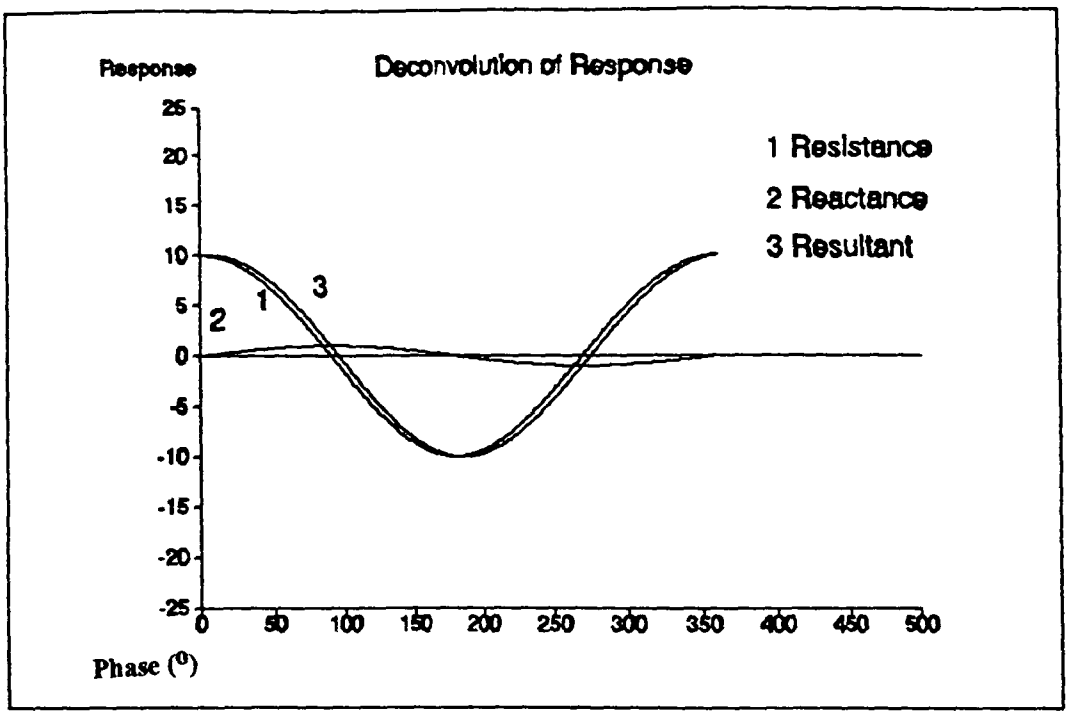

Figure 4.3. Deconvolution of the current response in terms of the two orthogonal contributions, resistance and reactance Note· in this case the resulting shape resembles mostly the resistive component The amplitude ratio used is reactance:resistance = 1:10

In the following experiment we tried to measure the capacitance of a diode in forward bias to see how badly this would affect the instrumentation The results of the reverse and forward bias scans made on the Au-GaAs diode will be presented in section 4.4 together with a possible solution to the problem of measuring capacitances accurately in the presence of high current densities

4 3 Preparation of the diodes

The diodes used have been prepared in the following fashion The overall procedure consists of three steps a) a chemical etch m order to obtain an oxide surface with a minimum of defects, b) fabrication of an ohmic (=non-rectifying) back-contact and finally c) the deposition of a metallic Schottky (=rectifying) contact

In order to obtain a native surface with a minimum of defects the samples are chemically etched using a $H_2SO_4/H_2O_2/H_20$ solution in a 5 1 1 ratio by volume for 2 minutes after the wafer had been degreased using acetone and methanol After rinsing in deionised water, an ohmic contact has been fabricated by applying an eutectic mixture of gallium and indium (GaIn) to the back and annealing in a gentle flow of dry nitrogen (to prevent oxidation) at 375 °C Finally, the Schottky contact was created by evaporating a thin gold film onto the semiconductor in vacuum (typical base pressure $1x10^{-8}$ Torr) A stainless steel mask with circular holes of 0 6 mm in diameter covered the semiconductor, resulting in the creation of evenly spaced Schottky diodes

4 4 Results obtained in reverse bias

The results obtained on the Au-GaAs diodes are presented in Figure 4 4. Two diodes located on a single wafer have been measured under reverse bias in the 10-100 kHz frequency region The two samples show consistent behaviour Apparently there is no frequency dependence in the range employed The results from the Mott-Schottky analysis (Figure 4 5, Equation 3 11) are within experimental error as compared to those obtained by using a Boonton capacitance meter

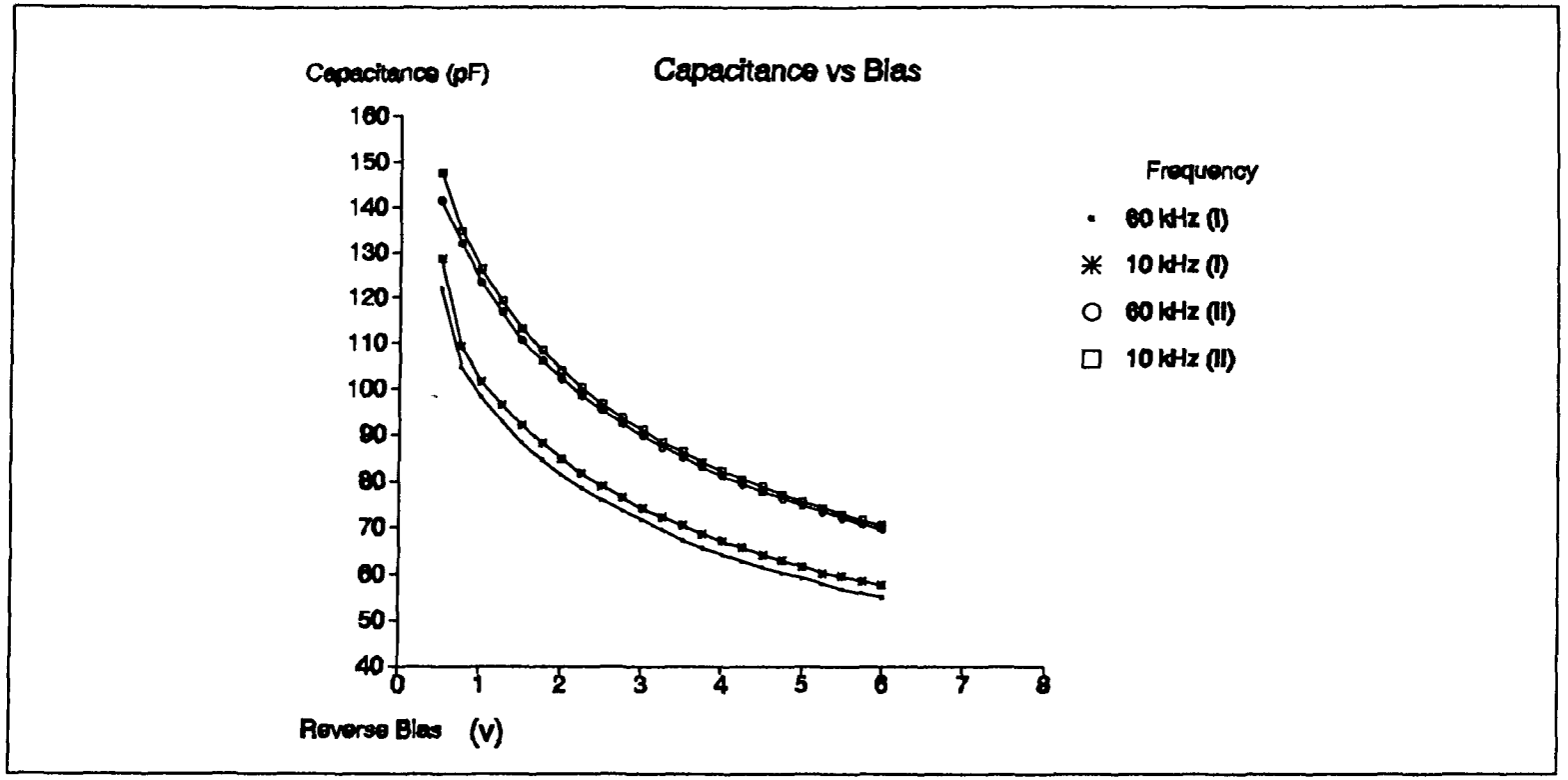

Figure 4.4. Capacitance versus reverse bias for two Au_GaAs diodes The results indicate the absence of frequency dependence for the 60-10 kHz region

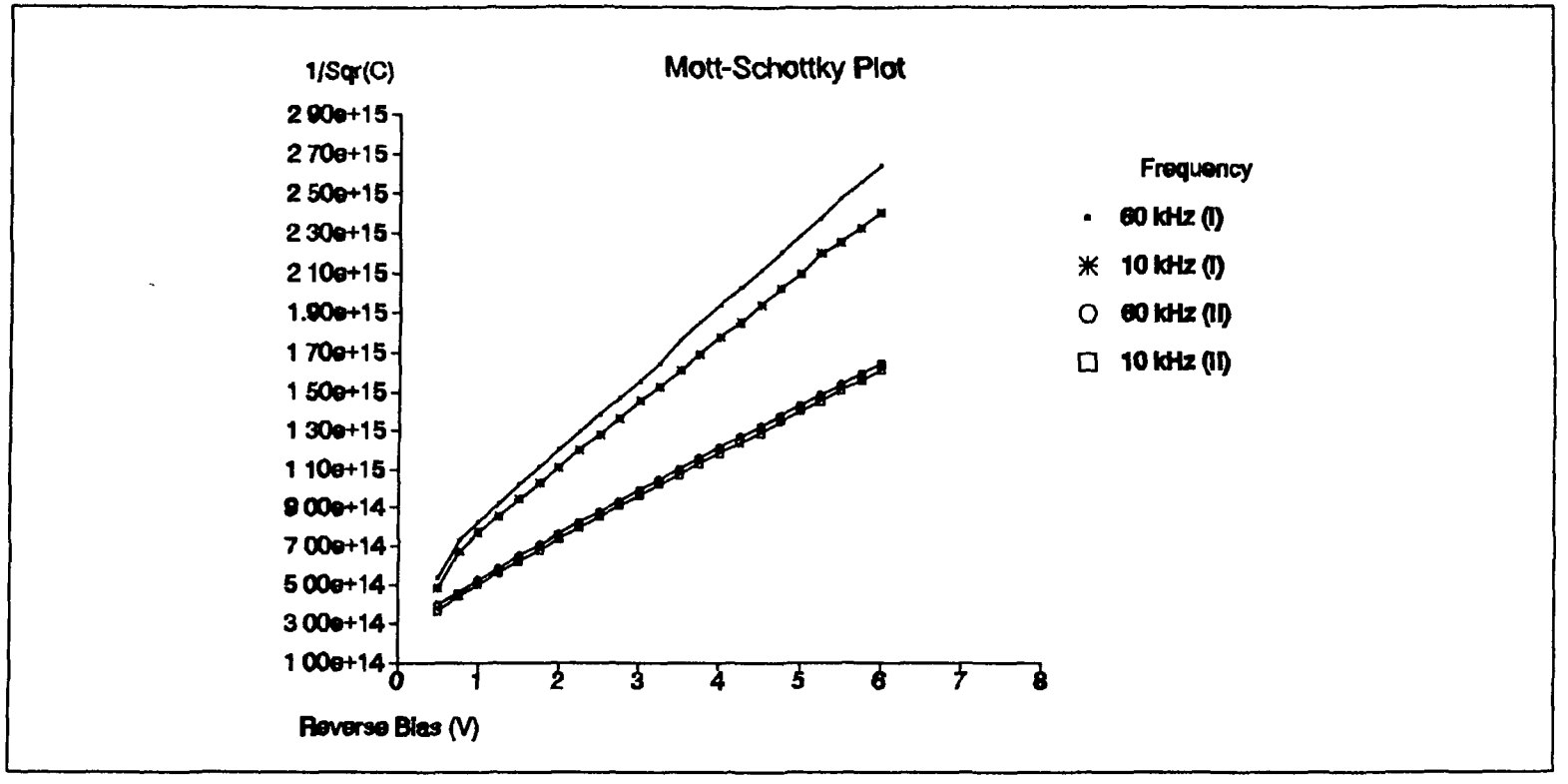

Figure 4.5. Mott-Schottky plots for the Au-GaAs diodes from data presented in Figure 4 4. From this plot the following parameters have been obtained doping density N_d=5±1 x 10^{16} cm^{-3}, flatband potential V_{fb} 1 2 ± 0 1 V using Equation 3 11.Dimensions of $1/C^2$ is $F^{-2}cm^4$.

4 5 Forward bias results

The same diodes have been submitted to capacitance measurements in forward bias When the forward bias is restricted to $0 \rightarrow 0.3$ V, rectifying behaviour is observed and values for the donor density and flatband potential are in agreement with those obtained reverse bias conditions ($N_d=3\pm1 \times 10^{16}$ cm^{-3}, flatband potential V_{fb} 1.0 ± 0.1 V). Again, at the frequencies employed there is no indication of a frequency dependence. On the other hand, if the forward bias is extended above 0 3 V, capacitances tend to become extremely large. This originates from two effects, a) the physical capacitance is increasing and b) the technique when used as described above is unable to deconvolute the current-to-voltage transducer output correctly. The latter is due to the fact that the resistive contribution to the current has become orders of magnitude larger than the capacitive component In Figure 4 6 (next page), a typical capacitance profile obtained at large forward bias is given A possible solution to this problem will be presented in the next section.

4 6 Accurate capacitance measurements in the presence of large current densities.

In the presence of large current densities, the deconvolution method used in the setup does not yield accurate results, as explained in the previous section There is an elegant solution to the problem of determining a small quantity (capacitive component of the current) in the presence of a much larger component (resistive current), if one can measure the combined signal at a particular phase where it is certain that the large component is zero [1] As can be seen from Figure 4 3, in this case the total signal S_t, which is given by Equation 4 2 (S_r and S_c are the capacitive and resistive components)

$$S_t = S_c + S_r \qquad (4.2)$$

If the phase is set at the particular angle where $S_r=0$ this results in S_t being equal to S_c and in this way gives direct access to the capacitive component without 'swamping' this with the much larger resistive component

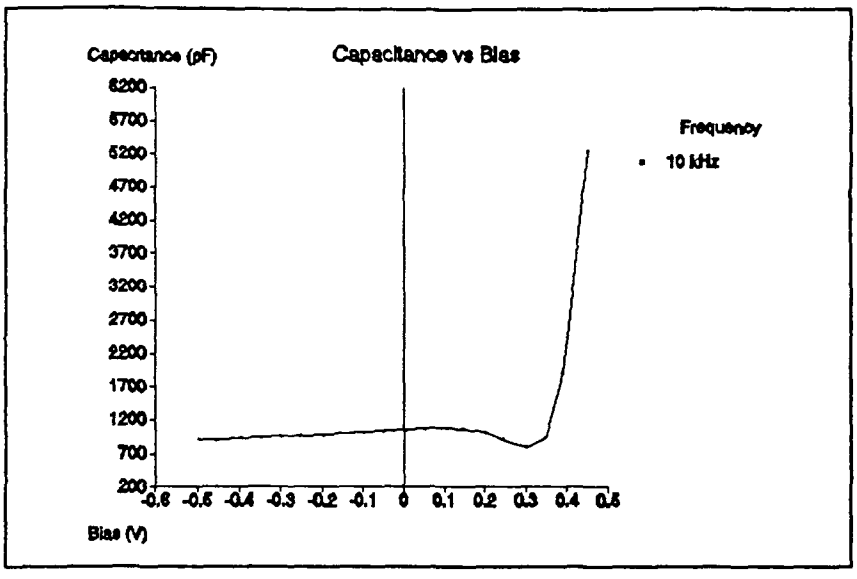

Figure 4.6. Capacitance versus large forward bias for one diode at 10 kHz. This demonstrates clearly the incapability of the technique to deconvolute the current-to-voltage signal properly for large current densities

This is achieved in the following manner, a test resistor of a size capable of changing the resistive components magnitude, is placed in parallel with the sample [1] The LIA is locked onto the current-to-voltage transducer output and if the set phase angle does not match the angle at which S_r passes through zero, the reading of the LIA will change significantly, and thus inform the operator of the fact that the phase is set incorrectly The phase is tuned while switching the parallel test resistor in and out of the circuit until there is no significant change in reading This reading is now equal to S_c, which represents the I_c and the capacitance is easily calculated using Equation 4 3 ($|V|$represents the RMS maximum magnitude of the modulation voltage V)

$$\frac{1}{\omega C} = \frac{|V|}{I_c} \qquad (4.3)$$

In this fashion, the capacitive component is directly accessible

Unfortunately, this elegant technique suffers from two drawbacks To null the S_r successfully if the signal is noisy, is not always straightforward and combined with the fact that if one is as little as 0 1° error in the setting of the phase while nulling S_r has dramatic effects

The resistive signal S_r is several orders of magnitude larger than S_c, and therefore when S_r is not nulled properly, the RMS reading of the LIA will not correspond to the purely capacitive component S_c, but will reflect a mixture of the resistive and capacitive contributions Because of this we were only capable of testing the technique on large commercial capacitors (around 1 μF) in which case S_c is not as easily swamped by the resistive response, even when the phase is not exactly set. On Au-GaAs diodes, where S_c is much smaller, we have not been able to make valid measurements

4 7 Bias profiles on Au-GaAs diodes at various temperatures (100-300 K)

The contribution to the capacitance from surface states and traps in a Schottky diode is temperature dependent, due the decrease in mobility of these specific ionic carriers, when lowering the temperature This 'freezing out' of surface states is employed in Deep Level Transient Spectroscopy amongst other techniques We would like to test our capacitance instrumentation to establish if we were able to detect such a change. In order to measure the capacitance profiles in the 100-300 K range the setup as described in section 3 9 has been modified to include a thermostated two-probe sample holder The sample holder was thermostated by using an Archimedes screw to transfer the nitrogen vapour in combination with a resistive heater fitted with a thermocouple, and a liquid nitrogen reservoir, all under vacuum maintained by a rotary pump The electronics as described in chapter 3 has been connected to this setup by two 20 cm coaxial cables, which introduces an expected stray capacitance of around 10 pF (commonly accepted is a stray of 60-70 pF/m coaxial cable used) A direct effect of lowering the temperature is the significant decrease in noise levels, probably due to a lowered contribution of thermal noise Because of noise problems we were restricted to using frequencies higher than 2 kHz

Apart from this observation, the capacitance measured did not exhibit a clear dependence on temperature At the chosen frequency (between 2 5 and 20 kHz) there was no trend visible, the values recorded at various temperatures between 100 and 300 K and at a range of frequencies, in both forward (0 → 0.55 V) and reverse bias (-1 → -5 5 V) lie within a standard deviation of 5-10 pF of each other

Therefore, from the data obtained in this preliminary experiment, it can be concluded that the sensitivity of the instrumentation as developed here is not sufficient to detect a change in capacitance due to 'freezing out' of the surface states traps by lowering the temperature over the 100-300 K range

4 8 Conclusions

The data obtained in these experiments show that our computer controlled capacitance measurement setup is a low-budget complement to the Boonton bridge arrangement which works well with a capacitance resolution in the order of picoFarads

References

1 H Evans, X Wu, E S Yang and P S Ho,
Appl Phys Lett , **46**, 486-488, 1985

Chapter 5

Presentation and discussion of preliminary results from the second phase of the project

5 1 Introduction

In this chapter an overview of the preliminary results measured during the second and third phase of this work as outlined in Chapter 1 will be presented As well the results from the electrochemical study of these materials as the surface analysis by means of STM and XPS of the redox-polymer on a glassy carbon substrate will be presented.

5 2 Surface analysis results

5 2 1. X-Ray Photoelectron Spectroscopy results.

X-ray photoelectron spectroscopy can determine both the individual elemental species present in a material and provides information on the range of chemical environments in which these elements exist Using a Kratos DS-800 series small spot size XPS spectrometer several core levels of cross linked Os-PVP material on glassy carbon disks have been investigated using Al Kα radiation (core levels: C(1s), O(1s), Os(4f), Br(3d), Cl(2p), S(2p) and N(1s) levels) Samples were mounted on metal stubs and transferred into a UHV environment for measurement Spectra were taken at a base pressure of 10^{-9} Torr or better and suitable peaks were fitted with a combined Gaussian and Lorentzian line shape (4/5 Gaussian + 1/5 Lorentzian) using the on-line analysis software of the DS-800.

The following samples were investigated:

a) native Os-PVP on glassy carbon substrate
b) as a) after cross link treatment
c) as b) soaked in 0 1 M sulphuric acid for 20 minutes
d) as b) cycled in 0 1 M sulphuric acid for 20 minutes
e) bare glassy carbon substrate

The C(1s) level of sample (e) is very broad and can be fitted to a combination of C=O, COH, and C and (C=O)OH features as shown in Figure 5 1. with a final fit value of 1. This is in agreement with the notion that the active surface of the glassy carbon is rich in oxygen.

With respect to the coated disks especially the S and N levels are of interest We hoped to distinguish between free nitrogen atoms, Osmium bound N and protonated N and to establish whether the sulphate anions would be bound as one or more bond specific species to the surface Unfortunately, various equally likely fits to the N(1s) bands obtained are possible including 2 or 3 species and after a rinse and vacuum dry (to remove loosely adsorbed sulphate from the surface) significantly different N(1s) spectra were obtained While no detailed deductions can be obtained from this particular set of data other than the fact that a number of the elements exist in different chemical environments, a more systematic approach from the point of view of film preparation may well provide more useful information. A system with less 'freedom' in terms of the number of variable components might be easier to study in this fashion

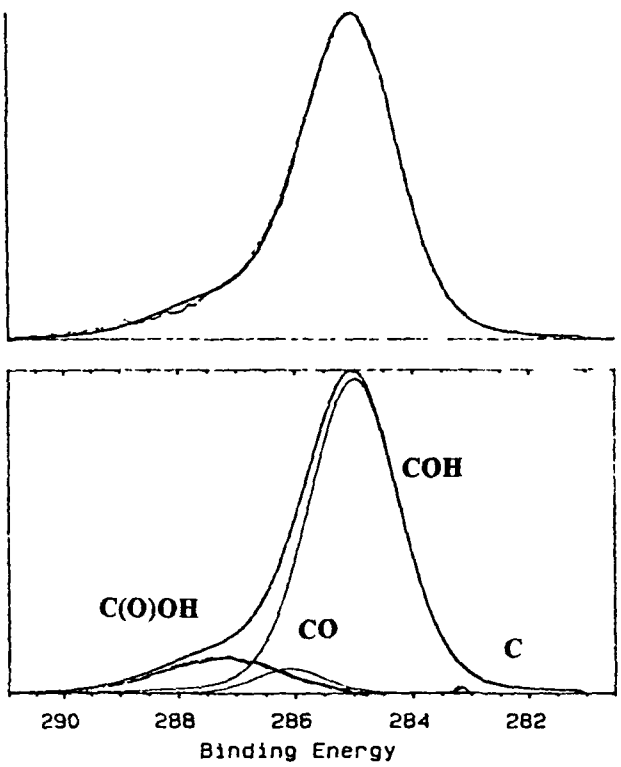

Figure 5.1. C(1s) Spectrum of the bare glassy carbon electrode showing the assignment of the chemically shifted C(1s) core levels (sample e).

5 2 2 Scanning Tunnelling Microscopy images

Several Scanning Tunnelling microscopy (STM) studies of the structure of a variety of conducting polymer layers have recently been reported The STM has the capability of providing three dimensional information on the surface morphology of a conducting material While it is technically feasible to image the polymer surface in an aqueous environment by using isolated tunnelling tips to image the sample, the images presented in this report are of dried films imaged in air. STM images of vacuum dried Os-PVP films deposited on either glassy carbon or Highly Oriented Pyrolytic Graphite (HOPG) substrates have been obtained using a Nanoscope II microscope. One reason for studying the form of the polymer film on a graphite surface is because of the highly ordered nature of this surface which can be well characterised prior to polymer deposition This allows the structure of the polymer layer to be determined independent of the substrate structure These preliminary studies seem to indicate that in the dry state there is no apparent order or long-range structure present at the polymer surface Some features of the experimental data taken will be presented in Figure 5 2-5 4.

Figure 5 2 Depicted is the 0 8x0 8μm STM image obtained using Nanoscope II equipment on a glassy carbon substrate The 7 mm glassy carbon substrate had been polished to a mirror finish employing 6 μm alumina slurry and 1 μm diamond paste as polishing agents This treatment resulted in an average roughness of the surface of less than 1 μm Note the score marks (from polishing) running at -45° with the horizontal axis

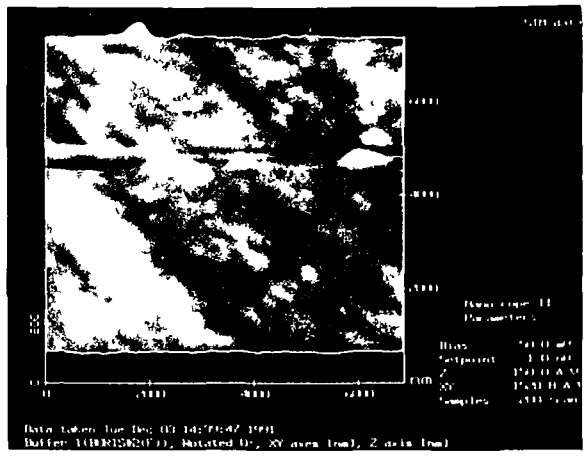

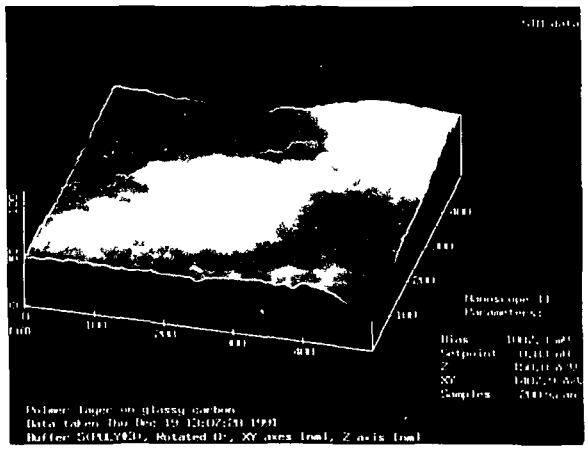

Figure 5 3 Shown is the image of an Os-PVP coating deposited onto the glassy carbon substrate The film has been dried *in vacuo* for 24 hours prior *to* the *measurement* No distinct structure can be assigned to the features visible in this image the polymer seems to be randomly dispersed over the entire monitored area of the substrate (0 5x0 5μm)

Figure 5 4 Electron density map for polymer material from the same batch on a HOPG substrate for a 0 1x0 1μm area (zoom-in from a 0 8x0 8μm scan) the HOPG substrate is known to form folds and ridges and the polymer chains seems to be clustered along these folds Apart from this physical alignment no formation of internal structures within the polymer can be seen

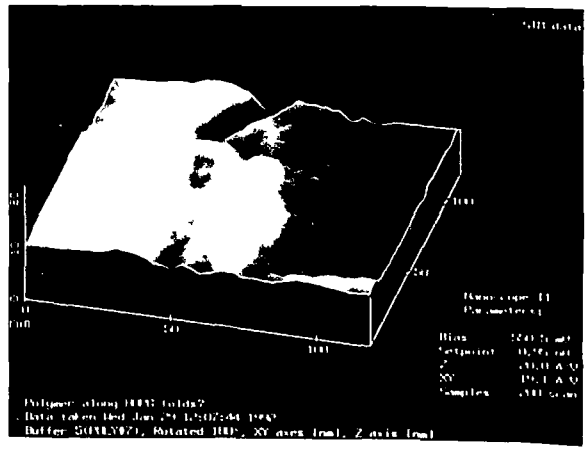

5 3 Overview of the electrochemical work

5 3 1 Background on the use of semiconductors as electrode material

The use of semiconductors for electrode materials may possibly yield additional information about the charge transfer mechanisms involved in redox reactions occurring at polymer modified electrodes, with respect to conventional studies employing electrodes exhibiting a metallic electronic character In these electrochemical experiments the electrode acts as a source (reduction) or sink (oxidation) of electrons and the charge transfer rate from the metal across the film interface is an intrinsic property over which one has no specific control

The electrical double layer at the electrode/electrolyte interface exists within 5 Å (Helmholtz layer), when a non-dilute electrolyte (typical concentration 0 1 mole/litre or higher) is used For a modified electrode (coated) the situation is similar, the difference being that the properties of the deposited film (*e g* counter-ions permeability) have an effect on the structure of the electrical double layer

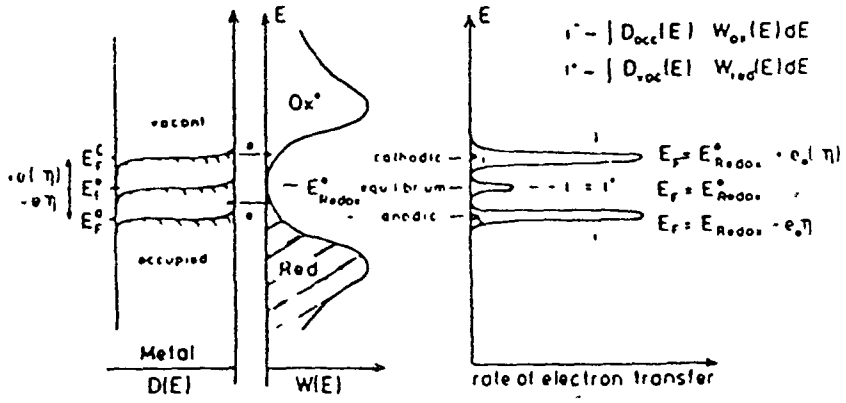

Figure 5.5. Diagram depicting the rate of electron transfer between a metal and a redox couple (see text for details) [1]

We will use the fluctuating energy model as proposed by H Gerischer [1] This model is based on the assumption that electroactive molecules possess an energy dependent on a energy level dictated by ionisation potential and electron affinities in combination with additional stabilising factors such as solvation energies or chelation energies. This energy level is consequently modulated by thermal fluctuations and the density of redox states as a function of energy E is given by Equation 5 1-5 2.

redox states as a function of energy E is given by Equation 5.1-5.2:

$$D(E) = \frac{[RED]}{\sqrt{(4\pi\lambda kT)}} \exp\left(-\frac{(E_r - E)^2}{(4\lambda kT)}\right) \qquad (5.1)$$

$$D(E) = \frac{[OX]}{\sqrt{(4\pi\lambda kT)}} \exp\left(-\frac{(E_o - E)^2}{(4\lambda kT)}\right) \qquad (5.2)$$

where λ is the reorganisation energy (difference between E_o or E_r and the Fermi level respectively) and all other symbols have their usual meaning. The charge transfer rate is determined by the overlap integral of D(E) and the electronic states in the electrode for the oxidised and reduced species respectively and the net current is controlled by the difference in these two rates.

In Figure 5.5. a schematic representation of the interaction between the Fermi level in the metal and the Fermi level of the redox couple, which coincides with the half wave energy ($0.5 \times (E_r + E_o)$), with respect to the energy of a free electron in vacuum. These energy levels are correlated with their respective redox potential V_x by $V_x := q(-4.5eV - E)$ in volts, and V_x being the redox potential versus the normal hydrogen reference electrode. The redox states are formally distributed around the oxidation and reduction potential respectively using a Gaussian distribution, according to R.A. Marcus, as described by Gerischer [1]. This implies that instead of only one possible energy level there exists a band of redox 'states'. The Fermi level of the metal is a function of applied potential and there are no forbidden regions. This type of interaction results in two distinct transfer currents above or below the Fermi level, in combination with a small exchange current at the equilibrium potential. Therefore, the model predicts an anodic and cathodic charge transfer rate, depending on the applied potential when a metal electrode is being used. With semiconductor materials the electrode also acts as an electron source or electron sink, but a very specific one. By using a semiconductor electrode the charge double layer is not restricted within the Helmholtz region but expands into the semiconductor material . A space-charge region (typical width 1000 Å) is formed across the semiconductor/electrolyte interface [2].

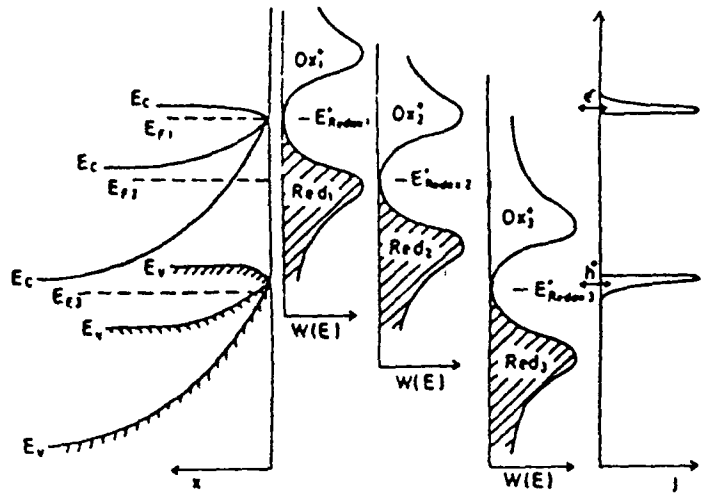

Figure 5.6. Diagram depicting the rate of electron transfer between three space charge regions and redox couples (see next page for details) [1].

The exchange current will be unidirectional due to the rectifying nature of the space-charge region, as will be outlined below. In Figure 5 6, three space-charge configurations for a n-type semiconductor are presented in conjunction with three possible redox couples and their relative energies If the Fermi level of the redox couple is located within the conduction band, an accumulation layer will be formed in order to align the Fermi levels in the equilibrium state Therefore, electrons are being made available at the surface and the result will be a considerable exchange of electrons

Similarly, if the Fermi level of the redox couple is located in the valence band an inversion layer will be formed in order to attain equilibrium and holes will be exchanged from the valence band Electron exchange from the conduction band is energetically unfavourable and therefore excluded and electrons located in the valence band are buried in the bulk and unavailable Therefore, after the initial exchange of holes, the electrode will become 'blocked' due to polarisation and external current will cease to flow, unless a considerable over-potential will be applied to 'unblock' the electrode

If the Fermi level of the redox couple is located with the band gap, a depletion region will be formed Due to the fact that electrons have moved away even further from the electrode surface, no exchange of electrons into the empty oxidised states is feasible

nor can electrons from filled reduced states reach the conduction band by thermal activation

5 3 2 Preliminary electrochemical results

Our system consisted of the redox polymer $[Os(bpy)_2(PVP)_{10}Cl]Cl$ (bpy=2,2'-bipyridine, PVP=poly-4-vinyl-pyrididine) on a glassy carbon or GaAs substrate in combination with a non-aqueous and aqueous electrolyte (0 1 molar tertiary butyl ammonium perchlorate in acetonitrile and 0 1 molar toluene sulphonic acid in water respectively) As outlined in Chapter 2 in more detail, due to the great importance of the interface in electrochemical processes, one would like to have direct control over the chemical and physical structure of the interface in order to be able to design this boundary on a molecular level As described in section 5.3 1 , the use of a semiconductor material will give additional control over the potentials at which charge transfer is possible. The modifying polymer layer restricts the potentials at which the charge can be transferred between electrode and electrolyte and if a semiconductor is used the relative position of the Fermi level of the redox couple located within the polymer with respect to that of the semiconductor dictates the direction of the net current at those restricted potentials We set out to study these devices using standard electrochemical equipment in combination with impedance spectroscopy using a set up similar to the one described in Chapter 3, the main difference being the use of a commercial potentiostat (EG & G 363) as a means of applying the modulation signal onto the electrochemical cell We choose a non-aqueous medium (acetonitrile) as electrolyte for our 'wet' applications, as water-based electrolytes would definitely result in oxidation of the semiconductor surface and a commercial $Ag/AgNO_3$ reference electrode was used

In semiconductor/liquid interface research, impedance spectroscopy is widely used to measure Mott-Schottky plots These plots yield information about doping level (slope) and flatband potential (x axis intercept) This flatband potential is the bias needed to null the band bending induced by the semiconductor/metal junction (Schottky diode) or semiconductor/electrolyte interface in the case of semiconductor electrodes and hence dependent on the properties of the interface.

The system was tested by measuring various RC circuits and by investigating a solid state Au-GaAs diode prepared as described in Chapter 4, but due to the lower sensitivity of the modified impedance set up, a large area diode was used In this case, the potentiostat was operated in two-electrode mode in air (reference electrode input and counter electrode input were interconnected and spring-loaded probes were used) Again the doping level of the material was verified using the Boonton capacitance bridge and our own AC impedance system The plot is presented in Figure 5 7 The results from the Boonton capacitance bridge and our own system were identical within experimental error The impedance spectroscopy technique gave N_D =5 5x10^{16} cm^{-3}, with a barrier height of 0 74 eV (correlation coefficient 0 9988) for this particular set of data The sample has been measured over a period of 3 days before it turned ohmic, possibly due to high currents passing through the sample All data sets acquired over this period of time were consistent

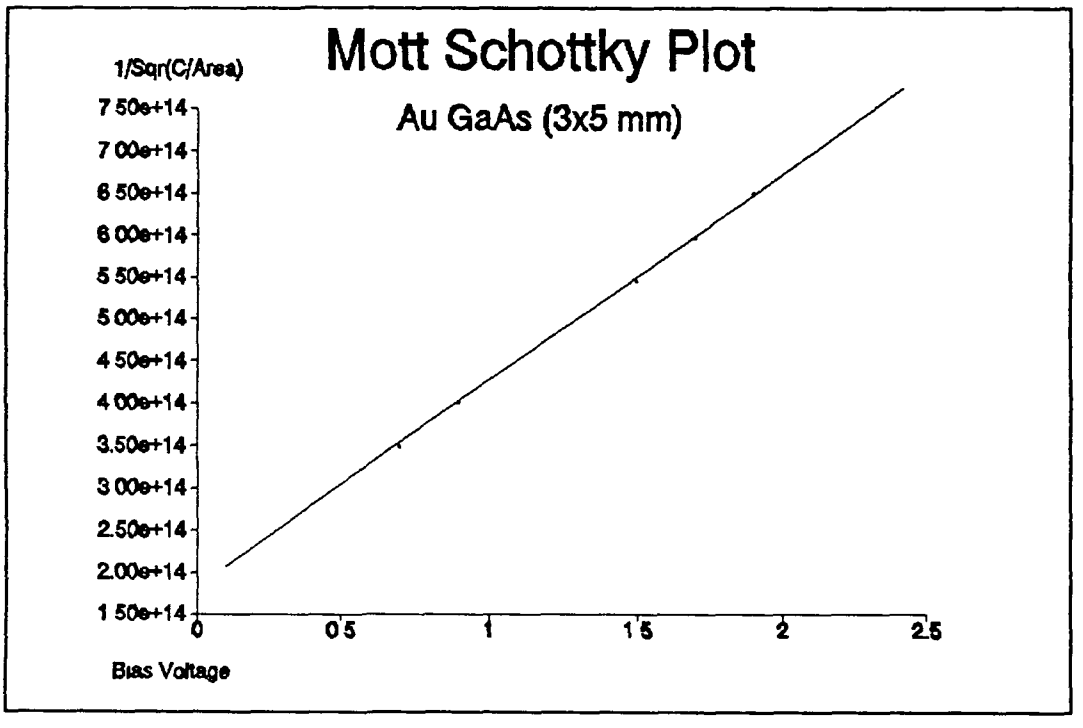

Figure 5.7. Mott-Schottky plot obtained on a 3 by 5 mm Au-GaAs diode in air using the modified impedance spectroscopy setup

If the usual size diodes were used (0 6 mm diameter Au dots on GaAs) the measured capacitances are in the order of 100-200 pF, under these conditions the presence of

N_D =1 4x10^{17} cm^{-3}, with a barrier height of 1 54 eV (correlation coefficient 0 9980). After correction for this stray capacitance (originating from the leads from the potentiostat) the following parameters were obtained N_D =4 5x10^{16} cm^{-3}, with a barrier height of 0 77 eV (correlation coefficient 0 9983) The Boonton capacitance bridge gave an N_D =5 2x10^{16} cm^{-3} value for the same diode The values obtained are typical for this type of diodes and based on these results the two systems are completely compatible, although the stray capacitance is less of a problem with the Boonton setup The modified impedance spectroscopy system using the potentiostat is capable of easily measuring large capacitances (up to 1 mF) and is hence suitable for the study of large area diodes

After the satisfactory completion of these tests, we tried to apply our system to semiconductor electrodes using GaAs with dopant concentrations of 10^{16}-10^{18} cm^{-3}, with acetomtrile as electrolyte. The conventional way of making semiconductor electrodes is to seal semiconductor squares into a glass tube using epoxy resin In our particular case epoxy resin was not suitable because of breakdown of these materials in the solvent used (acetonitrile) Therefore silicone rubber had to be used as a sealant Unfortunately, the use of silicone rubber introduced a delay of a day in the manufacturing of the electrodes and a high rejection rate (bad contacts or the front of the electrode contaminated with silicone) In order to be able to construct reliable electrodes more easily, a sample holder has been constructed out of Nylon using an O-ring seal and an screw action mechanism to clamp the sample down m combination with a spring-loaded contact This mechanism worked well, if clamped tight enough no leakage of the electrode could be detected However, while trying to measure Mott-Schottky data on the semiconductor/electrolyte junction (which should yield a similar barrier height as the Au-GaAs junction) problems occurred concerning the reproducibility of the data One of the problems was that samples tended to display ohmic instead of rectifying behaviour after some data sets had been obtained. Firstly, we considered the possibility that relatively high current densities passing through the sample at forward bias would force additional donors to enter the front of the sample hereby turning the rectifying contact into an ohmic one. However samples continued to turn ohmic within a few repeated bias ramps, even when the data was acquired under strict reverse bias conditions, when only relatively small currents are allowed

to pass through the samples (leakage current). Visual inspection showed that if bare GaAs had been used as electrode material, only minutes after immersion in the electrolyte (0.1 molar TBAP in acetonitrile), the typical blue metallic lustre of GaAs had been changed into a dull grey surface. This is possibly due to oxide formation enhanced by the acidic nature of the supporting electrolyte TBAP. When Au-GaAs diodes were used, it was possible to peel off the gold layer within minutes after the experiment had commenced. In some cases one could notice 'cracks' appearing in the gold coating. These observations are in agreement with observations reported elsewhere [3]. This, and the difficulties in mounting the semiconductor samples finally resulted in abandoning the use of the semiconductor GaAs as electrode material. A conventional substrate for the redox-polymers employed in this study is glassy carbon. The electrodes are made by melting carbon-rich materials such as petrochemicals in an oxygen free atmosphere.The resulting material is amorphous (unlike graphite), hence the term glassy carbon. The substrates used in this investigation are glassy carbon disks mounted in Teflon shrouds (7 mm diameter). The experiment was carried out as described in Chapter 2, and in order to verify and validate the software written, the previously studied system $[Os(bpy)_2(PVP)_{10}Cl]Cl$ (bpy=2,2'-bipyridine, PVP=poly-4-vinyl-pyrididine) on a glassy carbon, with 0.1 molar toluene sulphonic acid in water was used. Initial results were promising and in agreement with results found earlier by Dr. Robert J. Forster (Dublin City University), but persistent stability problems with the coatings forced us to leave this project as well. Some time ago, it became apparent the poor adhesion of the polymer was due to a poor quality glassy carbon.

5.4. Conclusions.

In the systems we have investigated, irreproducibility and/or instability of the polymer-electrode system causes major difficulties in studying these materials successfully using electrochemical and surface analysis techniques. We can however conclude from these studies that XPS and STM can be used to both determine the chemical composition and provide information on the film morphology. However, at least from these preliminary studies on this relatively complex system with four distinct components (metal centre, polymer, effect of electrolyte and substrate used) the results obtained show no significant trends or details, apart from a isomorph and random

appearance of the polymer Another reason for caution is that these surface analytical techniques suffer from a fundamental drawback when trying to correlate the electrochemical behaviour with the morphology of the film Preferably, the correlation should be made with the three dimensional (bulk) structure of the film, since both the heterogeneous and homogeneous charge transfer mechanisms are governed by a certain volume of film material. The polymer layer, which swells when solvated, provides a 3-D matrix within which the metal ions act as redox centres Surface techniques such as STM and XPS are capable of accurately determining surface properties. Therefore it is difficult to correlate kinetics, which are dictated by bulk material to a surface profile, which may or may not be a reconstructed reflection of the bulk structure The typical sampling depth of XPS is 2-3 nm in to the bulk while the polymer film can be microns thick Only when the surface structure is a true representation of the internal structure of the system, it is possible to use surface analysis data as obtained by XPS/STM to establish a correlation between charge transfer kinetics and morphology This shortcoming when generating a 2D profile of a 3D charge transfer process might account for the fact that considerable variations can occur in the XPS data without any significant change in the electrochemical activity of the layer.

References

1. H. Gerischer, Electrochimica Acta, 35, 1677-1699, 1990

2 S R Morrison, Electrochemistry at Semiconductor and Oxidized Metal Electrodes, Plenum Press, 1980

3. H O Finklea (editor), Semiconductor Electrodes, Elsevier,1988.

Chapter 6

Conclusions and suggestions for future work

6 1 Introduction

The three phases of the project as outlined in Chapter 1 have been described in the preceding 4 chapters of this thesis In this chapter a brief synopsis of each phase will be given, followed by suggestions for future work As has been stated in Chapter 1 the main objective of this project has been the design and implementation of software and/or hardware in order to enhance and facilitate measurement capabilities on existing electrochemical equipment and to build new instrumentation to provide us with a complementary technique to examine solid state devices in the form of variable frequency impedance spectroscopy. This has been accomplished in the first phase of the project and is outlined in Chapter 2,3 and 4.

These techniques in return have been used in an attempt to characterise the redox-polymer/semiconductor devices and its components The results of these preliminary investigations have been presented in Chapter 5, together with some surface analysis results using the scanning tunnelling microscope (STM) and X-ray photoelectron spectroscopy (XPS) respectively

As a result of the irreproducible nature of the devices combined with the time span of the project, the final step of the third phase, linking electronic/electrochemical behaviour of these materials with their morphology has not been achieved within the time-scale of this project

6 2 Phase 1 · implementation of PC based data acquisition and analysis systems

The instrumentation described in Chapter 2 and 3 is designed and build around a personal computer (PC) Not only facilitates this operation, data acquisition and analysis, but it also allows the experimenter to generate DeskTop Publishing quality diagrams directly from the 'raw' data Examples of this can be found in Chapter 4 and 5 Existing analogue equipment as in the case of the electrochemical equipment (Chapter 2) has been upgraded by adding digital processing power and PC-based control to the existing setup, while the usefulness of digital equipment has been greatly enhanced for the lock-in amplifier setup described in Chapter 3, by using a relatively inexpensive means of bidirectional communication (the serial port, RS-232) and a few in-house designed electronic add-ons

6 3 Phase 2 and 3 preliminary investigation of PME devices

As has been discussed in greater detail in Chapter 5, the electrochemical characterisation of the polymer modified electrode system (PME) used in this study, the redox polymer $[Os(bpy)_2(PVP)_{10}Cl]Cl$ (bpy=2,2'-bipyridine, PVP=poly-4-vinyl-pyrididine) on a glassy carbon or GaAs substrate in combination with a non-aqueous and aqueous electrolyte, proved to be troublesome. Reproducibility problems and a high failure rate of these PME's forced us to abandon this objective of the project. When trying to determine the morphology of the polymer film, the surface analysis techniques used were STM and XPS From the preliminary results presented in Chapter 5 it can be seen that the STM images depict a randomly distributed surface with no specific structural features and that the XPS results once again suffer from reproducibility problems and are at best inconclusive Apart from this, there is a more fundamental problem at hand when using a surface technique as a probe in order to study structural features which are possibly linked to a bulk process, such as charge transfer processes (also, see 5 4 1) Therefore we have proposed the use of a technique which acts as a local bulk probe, Extended X-Ray Absorbtion Fine structure Spectroscopy (EXAFS) This is a diffracting technique which provides information concerning the local environment of the scattering atom in the bulk The technique has a large penetration depth into the bulk due to fact that X-Ray photons are used for excitation The transmission (or absorbance) of these photons is studied as a function of energy and is based on the phenomena that the X-Ray absorbtion cross-section for an atom displays oscillations as a function of energy above the excitation threshold for a K or L shell electron These oscillations are caused by interference between the wave-functions of the outgoing electron excited by a high energy photon and those of electrons scattered by neighbouring atoms Therefore we would like to use this technique to investigate the local structure of the metal centre in the PME system studied As a first attempt we would suggest to study the polymer system itself in a solvent like methanol in oxidised and reduced form. We have successfully applied for beam-time at the Synchrotron Radiation Source in Daresbury (SRS, UK) under the Large Scale Facilities Scheme and have obtained a time slot in March 1993. The fine structure superimposed on the main threshold photon flux is analysed in the following manner After proper background correction for which there are various methods in use, the fine structure observed and that calculated for a likely structural model, are

compared and the model is adjusted until a proper fit and a physically plausible structure has been obtained One can design a structural model from scratch, but if available, diffraction data for suitable reference compounds to generate a diffraction profile is commonly used Crystallographic studies for such reference compounds containing a similar octahedral structure as the polymer material under study, containing 6 nearest neighbouring N atoms at 2 0 Å for the osmium and ruthenium metals respectively have been reported [1]. These reference compounds which have been synthesised in our laboratory possess a well documented local structure which is chemically only slightly different from the sites in the polymer (6 nitrogen atoms versus 5 N + 1 Cl atom respectively) They are therefore ideal model compounds on which to base our EXAFS investigations of the related polymer compounds Also it is possible to prepare sample solutions of the redox polymer and of the parent compounds which contain exactly the equivalent amount of metal centres, thereby rendering data sets from the parent compound and polymer readily comparable. We propose to study only sample solutions of the 1 10 and 1 5 ratio metal ligand loadings for the redox polymers in order to obtain relatively high intensity transmission signals concerning the back scattering properties of the nearest neighbours within the polymer. We propose to carry out the following experiments

1) compare the local structure of the catalytic metal centre in the polymers in solution with the first coordination shell of the parent compound

2) We would like to investigate the effect of redox state on bond lengths in the polymer systems in the liquid phase using EXAFS Eggleston et al. [2] have published the crystal structures of cis-Ru(2,2'-bipyridine)$_2$ moieties in the II and III redox state Apparently in the solid phase upon oxidation, the Ru-Cl bond is shortened by 0 10 Å while the Ru-N bond located trans from the Ru-Cl bond increases by 0 04 Å

3) Furthermore we would like to probe the effect of protonation of the unoccupied pyridine sites within the solvated polymer on the local structure of the metal centres

6 4 Final remarks

The main objective of this project has been the design and implementation of PC-based instrumentation, to facilitate the study of charge transfer processes occurring in PME's and diodes This phase of the project has been completed and all needed instrumentation has been validated as described in Chapter 2,3 and 4 Concerning phase 2 and 3 of the project, as discussed in the previous paragraphs and in Chapter 5, the present efforts to obtain consistent information concerning the electronic properties and structure of the redox polymer have been unsuccessful, partly due to reproducibility problems, which might be inherent to the relatively large number of sub-systems in the PME's (namely metal centre, polymer backbone, electrode substrate and supporting electrolyte) and partly due to the use of a technique like XPS, which might not be a prime candidate for this type of investigation

However, we feel that the use of a more suited technique to probe the local structure of the metal-centre, such as EXAFS might very well render useful information, especially when to number of components that make up the PME system is kept to a minimum (i e no substrate and no supporting electrolyte).

References

1. B D J R Fennema, R A G de Graaff, R Hage, J G Haasnoot, J. Reedijk and J G Vos, J Chem Soc Dalton Trans, 1991, 1043-1049

   M M Richter, B Scott, K.J. Brewer and R D Willet, Acta Chrystallogr , Sect C Cryst Struct Commun ,1991,C47(11), p 2441-2

2. D S Egglerton, K.A Goldsby, D.J Hodgson and T M. Meyer, Inorg Chem , 1985,24,4573-4580

Acknowledgements:

During the various stages of the project described in this thesis I received advice and help from people within the Chemistry and Physics Department I would like to acknowledge the following persons in particular for their contributions

I would like to thank Dr Greg Hughes for his support, patience and advice during the whole of the project The technical staff in both departments have been of great help, especially Theresa McDonnell, Peig Ward, Veronica Dobbyn and Fintan Keogh during my stay m Chemistry while developing the software described in Chapter 2. Also I would like to mention my liaison officer, Dr Han Vos

While working on the impedance spectroscopy I have been given hardware and electronics support from the following group of people Des Lavelle and Cian Merne, who designed manufactured the different prototypes sample holders, while Allen Hughes, Joe Maxwell and John Lynch built all circuit boards and gave advice on electronic matters Without the expertise of the above mentioned this project would have been much harder to complete. I am grateful to Al Devine for the photographic reproductions in Chapter 5

On the software front I am indebted to Robert Forster, Dr Dermot Diamond and Diarmud Corry for the suggestions and help offered during the development of the data acquisition software.

Philip Moriarty persistence in obtaining the Scanning Tunnelling Microscope images presented in Chapter 5 is kindly acknowledged Without his expertise on STM this would have been a macroscopic task

Also I would like to thank my fellow post graduates m Chemistry and Physics who helped me to keep the faith at times of desperation Two of those should not remain nameless my Daresbury synchrotron night-shift compamon (Dr ') Liam Roberts and Dave Kelly who accompanied me for the X-ray Photoelectron Spectroscopy experiments (Chapter 5) carried out in University of Ulster, Coleraine

Financial support from the EC (Science Plan # SC1000414) is gratefully acknowledged

Finally, I am indebted to Eithne for her support and common sense.

Appendix

Specifications RTI-815 I/O board

Function	Details	Resolution
Base Address	320 (hex)	
Board Type	815	
Analogue O/P	± 10 V	4.88 mV
Analogue I/P	± 5 V	2 44 mV
Coding	Binary	
Direct Memory Access	2000 Words	

Connections on break-out box for electrochemical work station

Function		Red (Hi)	Black (Lo)	Blue
O/P Trigger	Digital O/P	Pin A1	Pin A34	Pin A25
O/P Pulse	Analogue O/P	Pin B38	Pin B39	n a
I/P Channel 0	Voltage I/P	Pin B3	Pin B19	n.a
I/P Channel 1	Current I/P	Pin B5	Pin B21	n a

Note: A denotes Digital connector, B Analogue connector for the RTI-815

Electronic components used

lock-in amp circuitry

Revision 2.0

Materials

Item	Quantity	Reference	Part
1	7	J1..J7	BNC
2	3	R1,R2,R3	100K
3	1	R4	5K
4	2	U1,U2	TL081
5	2	U3,U4	CA3140
6	1	U5	DG419DJ

Low pass filter (100Hz)

Revision 1

Materials

Item	Quantity	Reference	Part
1	2	J1,J2	BNC
2	2	C1,C2	100 nF
3	2	R1,R2	15K
4	1	R3	27K
5	1	R4	47K
6	2	U1,U2	CA3140

Lock-in amplifier connections

Function	LIA BNC	BOX BNC (Jx)
Channel Switch	X6 Analogue O/P	Switch DAC I/P J7
LIA Input A	Input A	Switch O/P J6
Bias DAC	X5 Analogue O/P	Bias I/P J2
Bias ADC	X1 Analogue I/P	Bias O/P J3

Note: Jx denotes the BNC connection as depicted in the Electronic Schematics 3.9/3.10.